

Sparse OFDM: A Compressive Sensing Approach to Asynchronous Neighbor Discovery

Xu Chen*, Dongning Guo*, Gregory W. Wornell†

*Northwestern University, Evanston, IL, USA

†Massachusetts Institute of Technology, Cambridge, USA

Abstract

A novel low-complexity wireless neighbor discovery scheme, referred to as sparse orthogonal frequency division multiplexing (sparse-OFDM) is proposed. One area of application is the “Internet of Things” (IoT). The number of devices is very large while every device accesses the network with a small probability, so the number of active devices in a frame is much smaller than the total local device population. Sparse OFDM is a one-shot transmission scheme with low complexity, which exploits both the parallel channel access offered by OFDM and the bursty nature of transmissions. When the transmission delay of each device is an integer number of symbol intervals, analysis and simulation show that sparse OFDM enables successful *asynchronous* neighbor discovery using a much smaller code length than random access schemes.

I. INTRODUCTION

By some estimate [1], there will be more than 200 billion sensor enabled objects world-wide in the Internet of Things (IoT) by year 2020. There can be over a million such devices within 500 meter range in a densely populated area. For any wireless device to function in the IoT or an ad hoc network, the first step is to discover access points and/or other communication parties within range and also be discovered by them. This is called neighbor discovery.

Neighbor discovery is an essential step for medium access protocols and routing protocols. There has been a large body of research works on neighbor discovery for general networks [2]–[4]. In conventional networks, the overhead of neighbor discovery is often thought of as amortized over the long data transmission. However, a typical IoT device makes bursty transmissions and the message is usually short in a single transmission. It has been shown that the neighbor discovery overhead may considerably reduce the data throughput in systems involving a massive number of devices [5]. It is critical to minimize the neighbor discovery overhead.

Due to its unique features, the IoT poses additional challenges for designing an ultra-scalable scheme [6]. The total number of IoT devices is extremely large and it is hard to achieve perfect synchronization. Many IoT devices are of low cost and low power. A scalable scheme should have relatively low computational complexity at the device side.

The current technology and protocols may be inadequate to address the challenges. For example, a naive time division multiple access (TDMA) scheme to schedule all the devices would incur too much latency. Neighbor discovery using conventional multiuser detection approaches, say code division multiple access (CDMA) or orthogonal frequency-division multiple access (OFDMA), generally involves a complexity that scales polynomial in the number of devices [4], which is also unaffordable considering the large latency and power consumption. In this paper, we propose an efficient neighbor discovery scheme that tackles the above-mentioned issues.

A. Related Work

Network layer approaches: Network layer protocol designs for neighbor discovery can be categorized into randomized and deterministic algorithms. The main objective is to optimize random access probability or the transmit schedule of each device such that the system throughput is maximized [2], [3], [7]–[9]. Instead of purely avoiding collision, the FlashLinQ technology developed by Qualcomm assigns channels based on signal-to-interference ratios and achieves superior performance over carrier sense multiple access with collision avoidance (CSMA/CA) systems [10], [11]. The neighbor discovery algorithm proposed in this paper can be regarded as a physical layer technique, which can be optimized with the network layer protocols to improve the system performance.

Coded random access: Recently, the idea of codes on graph has been applied in random access [12], [13]. One scheme is named coded slotted ALOHA, where the packets are repeatedly transmitted in different slots and are decoded using successive cancellation. These works assume synchronization transmission and perfect interference cancellation. The asynchronous model has been studied in [14]–[16], where the asynchronicity is modeled to cause additional interference. However, perfect interference cancellation was still assumed. Rateless codes have been proposed for multiple access in machine-to-machine communications [17], where the channel gains are assumed to be known. As the number of users increases, the imperfect channel estimation is detrimental to the performance of successive cancellation.

In common with coded slotted ALOHA, our neighbor discovery scheme also applies erasure correcting codes to design the successive cancellation framework. Our proposed scheme differentiates itself in different aspects. In particular, our scheme is a one-shot transmission. Moreover, we carefully characterize the error propagation effects due to residual channel estimation error.

Multi-user detection approaches: Neighbor discovery can be formulated as multiuser detection from the perspective of physical layer processing [4]. Due to the bursty traffic patterns, the number of active devices is typically orders of magnitude smaller than the total local device population. Based on this crucial observation, low-complexity neighbor discovery algorithms inspired by compressed sensing were proposed [18]–[22]. These algorithms can reduce the code length by over 50% compared with the 802.11 type protocols, but they require synchronous transmissions. The LASSO algorithm was proposed to detect active devices in asynchronous CDMA random access [23], but it involves a high complexity when the total number of devices is large. In particular, its computation complexity scales polynomially with the total number of devices. Ideally, the complexity of a desirable scheme only scales polynomial with the number of active users.

Group testing: Noncoherent neighbor discovery based on energy detection can be formulated as the classical group testing problem [24]. By utilizing the sparsity nature, neighbor discovery can be achieved efficiently using a low transmission overhead. A related study applies sparse graph codes to asynchronous group testing [25], where the required code length is larger than that for our proposed scheme.

B. Contributions

In this paper, we propose a novel scheme, referred to as sparse orthogonal frequency-division multiplexing (sparse-OFDM), for *asynchronous* neighbor discovery. A key feature that distinguishes the proposed scheme from previous schemes is that sparse OFDM exploits both the parallel channel access enabled by OFDM and the bursty transmission nature in the IoT. Specifically, sparse OFDM judiciously allocates the sparsely separated channels to the devices. The resulting signal structure relates neighbor discovery to the sparse Fourier transform, studied in, e.g., [26], which applies to time-domain signals whose Fourier transform domain representation is sparse. The main features of sparse OFDM are as follows:

- 1) When the number of active devices and the maximum delay in terms of sample points is sublinear relative to the device population, sparse OFDM can correctly detect the active devices with high probability. It only requires sublinear computational complexity and a sublinear number of transmit symbols in terms of the device population.
- 2) Sparse OFDM is a one-shot transmission as opposed to scheduling the devices to transmit many frames in random access protocols. It utilizes the low-complexity point-to-point capacity-approaching codes, while at the same time exploits the multiuser diversity from successive cancellation.
- 3) Sparse OFDM is inspired by the recent development of the sparse Fourier transform [26] and sparse Hadamard transform [27]. The previous works assume the signal amplitudes belong to a known discrete alphabet, and the signal amplitude can be perfectly recovered [26], [28], [29]. In this paper, we assume arbitrary signal amplitudes, and characterize the effect of error propagation due to imperfect signal estimations leveraging the results on random hypergraphs.
- 4) Sparse OFDM provides practical physical-layer capability for multipacket reception. The scheme can be jointly designed with the random access protocol to further optimize the performance [30], [31]. Moreover, sparse OFDM can be easily adapted to the case of peer-to-peer broadcasting, where each device has multiple bits of information to send. Sparse OFDM is particularly appealing in the IoT, where a typical message is short.

C. Paper Organization

The rest of the paper is organized as follows. Section II presents the system model and main results. Section III describes the signalling scheme of sparse OFDM. Section IV presents the asynchronous neighbor discovery algorithm. Section V and Section VI provide proofs of the theoretical performance guarantees for synchronous and asynchronous transmission, respectively. Section VII presents the numerical results. Section VIII concludes the paper.

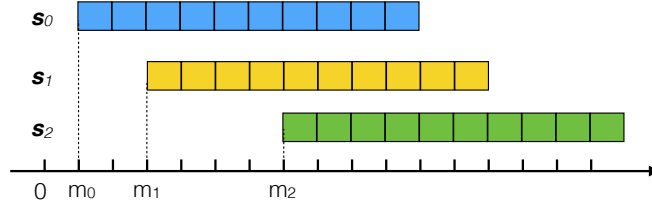


Fig. 1: Frame-asynchronous symbol-synchronous three-user model.

Throughout the paper, the index of a vector or each dimension of a matrix starts from 0. The elements of a $B \times C$ matrix are denoted as y_b^c , where $c = 0, \dots, C-1$ and $b = 0, \dots, B-1$. We write the b -th row vector as $\mathbf{y}_b = (y_b^0, \dots, y_b^{C-1})$ and the c -th column vector as $\mathbf{y}^c = (y_0^c, \dots, y_{B-1}^c)$. We denote the real and imaginary parts of a variable X as X_R and X_I , respectively. All logarithms are base 2.

II. SYSTEM MODEL AND MAIN RESULTS

Consider a network with N devices in total. Let $\mathcal{K} \subseteq \{0, \dots, N-1\}$ denote an arbitrary set of active devices, and $K = |\mathcal{K}|$ is the number of active devices. We assume symbol synchronicity without frame synchronicity, i.e., the delay of each device's transmission is an integer number of symbol intervals. Fig. 1 shows the three-user model. Moreover, the delay of any device is no greater than M symbol intervals due to propagation delay and clock/timing differences between the transmitting and receiving devices. To yield scalable results, we let both the number of active devices K and the maximum delay M scale up with N as $N \rightarrow \infty$ in general. We assume all the devices are aware of a reference frame start point of their neighbors. This can be easily achieved by using a common beacon signal. Device k transmits an L -symbol codeword, described as $s_{k,0}, \dots, s_{k,L-1}$. It suffices to consider a single receiver and its discovery problem. In the absence of frequency selectivity, the received signal at every (integer) time i is given by

$$x_i = \sum_{k \in \mathcal{K}} a_k s_{k,i-m_k} + w_i, \quad (1)$$

where $a_k \in \mathbb{C}$ is the channel coefficient, m_k is the transmission delay of device k , and w_i are independently and identically distributed (i.i.d.) circularly symmetric complex Gaussian random variables with distribution $\mathcal{CN}(0, 2\sigma^2)$. The discovery scheme is based on signals within a single codeword duration. From each receiver's point of view, the signal $s_{k,i} = 0$ for $i < 0$ and $i \geq L$ for all k .

We shall design a transmission and detection scheme with small code length and low computational complexity. Each codeword is appropriately designed so that the code length L is sublinear in N when K and M are sublinear in N . The following two theorems are the key results of this paper:

Theorem 1: Suppose the device transmissions are perfectly synchronized to the receiver's frame, i.e., $M = 0$. Suppose the noise variance is fixed and the channel amplitudes of all active devices is at least \underline{a} . For every $\underline{a}, \epsilon > 0$, there exist $\alpha_0, \alpha_1, K_0 > 0$ such that for every N and K satisfying $N \geq K \geq K_0$, there exists a code of length $L \leq \alpha_0 K \log N$, such that $\mathbb{P}\{\hat{\mathcal{K}} \neq \mathcal{K}\} \leq \epsilon$ for every subset \mathcal{K} of active users of size not larger than K , where $\hat{\mathcal{K}}$

is the estimated set of active devices. In addition, the number of arithmetic operations needed for computing $\hat{\mathcal{K}}$ is no greater than $\alpha_1 K (\log K) (\log N)$.

Theorem 2: Suppose the transmission delay of each device is an integer number of symbol intervals upper bounded by M . Suppose the noise variance is fixed and the channel amplitude of every active device lies in the region of $[\underline{a}, \bar{a}]$. For every $\underline{a}, \bar{a}, \epsilon > 0$, there exist $\alpha_0, \alpha_1, K_0 > 0$ such that for every N and K satisfying $N \geq K \geq K_0$, there exists a code of length $L \leq \alpha_0 ((K + M) \log N + K \log(K + M))$, such that $\mathbb{P}\{\hat{\mathcal{K}} \neq \mathcal{K}\} \leq \epsilon$ for every subset \mathcal{K} of active users of size not larger than K , where $\hat{\mathcal{K}}$ is the estimated set of active devices. In addition, the number of arithmetic operations needed for computing $\hat{\mathcal{K}}$ is no greater than $\alpha_1 K ((\log K) (\log N) + KM \log(K + M))$.

Theorem 1 and Theorem 2 provide the scaling of complexity and code length in terms of the device population and the number of active devices to achieve reliable device identification. Synchronous neighbor discovery, i.e., $M = 0$, requires a smaller code length and fewer arithmetic operations than the asynchronous case. In both theorems, a lower bound on the signal strengths is needed for successful sparse recovery [32]. In a practical system, if the channel gain between two devices is too small, they are not regarded as neighbors of each other.

The maximum relative delay M is usually small in practice. The delay depends on the timing difference and the maximum distance between a device and the receiver. For example, a distance of 300 meters implies free space propagation delay of one microsecond, which spans 20 samples if the sampling frequency is 20 MHz. Suppose the maximum delay M is constant. When the number of active users K is sublinear in terms of the device population N , i.e., $K = o(N)$, the code lengths for both the synchronous and asynchronous schemes are sublinear in the number of devices. When $K = o(\sqrt{N})$, the number of arithmetic operations involved in the asynchronous scheme is also sublinear in N .

III. SPARSE OFDM SIGNALING

Our scheme inherits the idea of OFDM. OFDM divides the spectrum into multiple orthogonal frequency bins, which are assigned to different devices for transmission. In conventional OFDM, we need at least N orthogonal frequency bins if we want to schedule the transmission of all N devices at the same time. In the case of assigning N orthogonal frequency bins, every OFDM symbol consists of N samples in the time domain. If the number of devices is large, the frequency bins will be narrowly spaced and correspondingly the OFDM symbol incurs a long code length. In our proposed scheme, the spectrum is instead divided into $B \ll N$ sparsely spaced frequency bins. The scheme is thus referred to as sparse OFDM. It will be seen that sparse OFDM will have a short code length and small computational complexity.

In the following, to facilitate the exposition, we will describe our signaling scheme in three steps. First, we consider noiseless neighbor discovery where the total device population N is smaller than the number of available OFDM frequency bins B . Second, we consider noiseless neighbor discovery where $B < N$ and a single device is active. Third, we consider the general noisy neighbor discovery, where $B < N$ and $1 < K \ll N$ devices are active.

A. Device Identification in the Case of $B \geq N$

The key idea for addressing arbitrary delay is to use the fact that the frequency of a sinusoidal signal is invariant to delay, where the delay merely causes a phase shift. Since the channel incurs an arbitrary delay that is bounded by M , we include M samples in the OFDM symbol as a cyclic prefix. Each OFDM symbol contains $B + M$ samples. Since $N \leq B$, we can choose a discrete frequency $b_k \in \{0, \dots, B - 1\}$ to uniquely identify device k . One way of assigning unique frequency bin is to assign the bins according to the device index, i.e., $b_k = k$. The discrete-time signal structure is given by

$$s_{k,i} = g_k \exp\left(\frac{j2\pi b_k i}{B}\right), \quad i = 0, \dots, B + M - 1, \quad (2)$$

where $g_k \in \mathbb{R}$ is a known design parameter of unit amplitude.

At the receiver side, the signals from all the neighbors arrive after a reference frame start point. The receiver discards the first M samples of each sparse OFDM symbol and collect the remaining B samples as $\mathbf{y} = (y_0, \dots, y_{B-1})$, where $y_i = x_{i+M}$, $i = 0, \dots, B - 1$. If each device is assigned a unique tone, performing B -point discrete Fourier transform (DFT) on \mathbf{y} yields a tone at the b_k -th frequency bin if and only if device k is active. Therefore, the signaling scheme (2) is sufficient to detect the active devices in a noiseless case with computational complexity of $O(B \log B)$ needed by the Fast Fourier Transform (FFT) algorithm. The delay m_k only affects the phase of the DFT value, so we can uniquely identify the user based on its frequency. This important insight will lead to the signaling design for a general case.

B. Single Device Identification in the Case of $B < N$

Suppose there are $N > B$ devices and only a single device k is transmitting under the noiseless setting. In this case, it is impossible to assign a unique frequency bin to each device. Instead, we randomly assign one out of B bins to every device. We still apply the signaling scheme give by (2). Suppose performing B -point DFT on \mathbf{y} yields a tone at the b -th frequency bin, we still cannot identify which device is active, because there may be multiple devices assigned to this bin due to random binning. The way to resolve this problem is to transmit multiple OFDM symbols and embed the device information through coefficient g_k in (2).

Let $C = \lceil \log N \rceil$ and $(k)_2 = (k_1, \dots, k_C)$ denote the binary representation of device index k . We design $(g_k^0, \dots, g_k^C) = (1, (-1)^{k_1}, \dots, (-1)^{k_C})$. We apply the signaling scheme (2) to $C + 1$ OFDM symbols, with the c -th symbol having $g_k = g_k^c$ in (2). In particular, we let device k transmit (s_k^0, \dots, s_k^C) , where $s_k^c = (s_{k,0}^c, \dots, s_{k,B+M-1}^c)$ and

$$s_{k,i}^c = g_k^c \exp\left(\frac{j2\pi b_k i}{B}\right), \quad (3)$$

for $i = 0, \dots, B + M - 1$ and $c = 0, \dots, C$. The code length is thus $(C + 1)(B + M)$ samples. For every c -th OFDM symbol, we discard the first M samples and the last B samples form a vector $\mathbf{y}^c = (y_0^c, \dots, y_{B-1}^c)$, where

$y_i^c = x_{i+c(B+M)+M}$, $i = 0, \dots, B-1$. Performing B -point DFT on y^c yields

$$Y_b^c = \frac{1}{B} \sum_{i=0}^{B-1} \exp\left(-\frac{\iota 2\pi b i}{B}\right) y_i^c \quad (4)$$

$$= \sum_{k \in \mathcal{K}: b_k = b} A_{k,b} g_k^c, \quad b = 0, \dots, B-1, \quad (5)$$

where

$$A_{k,b} = a_k \exp(\iota 2\pi b(M - m_k)/B). \quad (6)$$

As in the $B \geq N$ case, the delay m_k only affects the phase of the frequency value of the received signal from device k . The frequency binning effectively separates the devices.

Thus, each frequency bin b is associated with a length- $(C+1)$ vector $\mathbf{Y}_b = (Y_b^0, \dots, Y_b^C)$. It can be seen that g_k^0 serves as a reference symbol capturing the channel coefficients. In our setting, $Y_b^0 = A_{k,b}$. Therefore, the j -th bit of the binary representation of k can be estimated as $k_j = 0$ if $Y_b^{j+1}/Y_b^0 = 1$ and $k_j = 1$ if $Y_b^{j+1}/Y_b^0 = -1$.

The two design parameters b_k (frequency) and g_k (gain) play important roles. In particular, g_k is used to carry the device index information. The frequency b_k is designed to separate devices into different frequency bins. By design, the relationship between the device index and its transmit frequency is represented by a bipartite graph. In the bipartite graph, the devices represent left nodes and the B frequency bins represent right nodes. Left node i is connected with right node j if device i transmits at the j -th frequency bin. We call a frequency bin a *zeroton*, *singleton* or *multiton*, if no device, a single device, or more than one device transmit at the frequency tone, respectively. Fig. 2 illustrates an example of bipartite graph with a total of $N = 4$ devices, $K = 3$ active devices, and $B = 5$ frequency bins. In the example, bin 0, 1 and 4 are zeroton bins, bin 3 is a singleton bin and bin 2 is a multiton bin.

When there is a single active device in the noiseless setting, the signaling of sparse OFDM consists of $\lceil \log N \rceil$ OFDM symbols. Therefore, the active device can be identified with code length of $O((B+M) \log N)$ samples and computational complexity of $O(B(\log B)(\log N))$.

C. Identification of Multiple Active Devices With and Without Noise

When multiple devices are active, the active devices may use colliding tones, so that the device information cannot always be directly recovered from $Y_{b_k}^{j+1}/Y_{b_k}^0$, $j = 0, \dots, \lceil \log N \rceil$. The idea is to let the devices transmit at *multiple* frequency bins. As in the case of a single active device, we first identify active devices from the singleton bins. The identified device information is then used to bootstrap the detection of other devices.

The presence of noise raises additional questions: 1) How can we reliably estimate the channel coefficients? 2) How can we robustly estimate the device information in the noisy setting? 3) How can we distinguish a frequency bin to be a zeroton, singleton or multiton? In the following, we further enhance the signaling scheme to address these three challenges. Specifically, the overall frame structure is described in Fig. 3. The frame structure contains two subframes. The first subframe is used for device identification and the second subframe is used for synchronization.

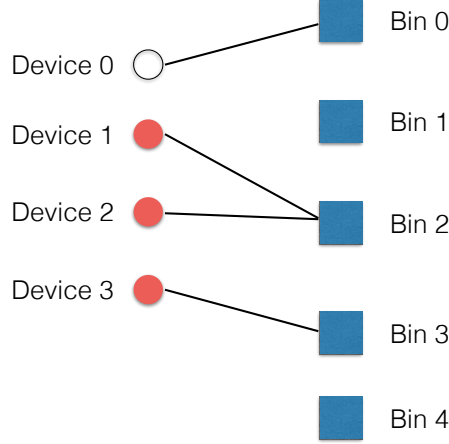


Fig. 2: Bipartite graph representation of sparse OFDM. Left nodes represent devices and right nodes represent frequency bins. The active devices are marked in red. Bin 0, 1 and 4 are zero-ton bins, bin 3 is singleton bin, and bin 2 is multi-ton bin.

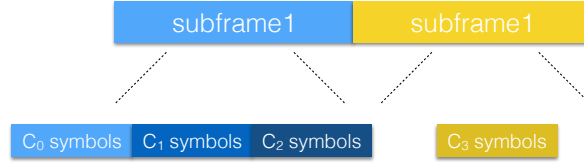


Fig. 3: Frame structure of sparse OFDM. A frame consists of two subframes, where the first subframe contains $C_0 + C_1 + C_2$ OFDM symbols and the second subframe contains C_3 OFDM symbols.

Signaling for the first subframe: We first introduce the signaling of the subframe used for device identification. The subframe consists of three segments and the i -th segment consists of C_i OFDM symbols, $i = 0, 1, 2$. Every device transmits $C = C_0 + C_1 + C_2$ OFDM symbols. For every OFDM symbol, device k is assigned to a fixed set of $\mathcal{B}_k \subseteq \{0, \dots, B-1\}$ frequency bins. In particular, we let device k transmit (s_k^0, \dots, s_k^C) , where $s_k^c = (s_{k,0}^c, \dots, s_{k,B+M-1}^c)$ and

$$s_{k,i}^c = g_k^c \sum_{b_k \in \mathcal{B}_k} \exp\left(\frac{j2\pi b_k i}{B}\right), \quad (7)$$

for $i = 0, \dots, B+M-1$ and $c = 0, \dots, C$.

For the c -th OFDM symbol, as in the previous cases, we discard the first M samples and obtain the remaining B samples as \mathbf{y}^c . Under the noisy setting, performing B -point DFT on \mathbf{y}^c yields

$$Y_b^c = \sum_{k \in \mathcal{K}: b \in \mathcal{B}_k} A_{k,b} g_k^c + W_b^c, \quad b = 0, \dots, B-1, \quad (8)$$

where $A_{k,b}$ is given by (6), and W_b^c are i.i.d. complex Gaussian variables with distribution $\mathcal{CN}(0, 2\sigma^2/B)$.

Let the length- C design vector for device k be

$$\mathbf{g}_k = \begin{bmatrix} \mathbf{1} \\ \tilde{\mathbf{g}}_k \\ \dot{\mathbf{g}}_k \end{bmatrix} \quad (9)$$

where the all-one vector $\mathbf{1}$ of length C_0 , $\tilde{\mathbf{g}}_k \in \mathbb{R}^{C_1}$ and $\dot{\mathbf{g}}_k \in \mathbb{R}^{C_2}$ are the design vectors for the first C_0 OFDM symbols, the second C_1 OFDM symbols, and the remaining C_2 OFDM symbols, respectively. The DFT values at the b -th bin \mathbf{Y}_b is a vector of length C and can be written as

$$\mathbf{Y}_b = \begin{bmatrix} \bar{\mathbf{Y}}_b \\ \tilde{\mathbf{Y}}_b \\ \dot{\mathbf{Y}}_b \end{bmatrix} \quad (10)$$

$$= \sum_{k \in \mathcal{K}: b \in \mathcal{B}_k} A_{k,b} \begin{bmatrix} \mathbf{1} \\ \tilde{\mathbf{g}}_k \\ \dot{\mathbf{g}}_k \end{bmatrix} + \begin{bmatrix} \bar{\mathbf{W}}_b \\ \tilde{\mathbf{W}}_b \\ \dot{\mathbf{W}}_b \end{bmatrix}. \quad (11)$$

The design vector is inspired by the generalized low-density parity-check (LDPC) framework for sublinear compressive sensing [33]. The detailed construction of these vectors will be elaborated later. From a high level perspective, the first all-one segment is used for robust estimation of the channel coefficients. The second segment is used to encode the device index information. With the first two segments, the active device indices can be estimated. However, a false alarm may occur. The last segment is used to avoid possible false alarms.

In the absence of noise, we let $\tilde{\mathbf{g}}_k = (1, (-1)^{k_1}, \dots, (-1)^{k_{\lceil \log N \rceil}})$, which carries the device information. Under the noisy setting, the values of $\tilde{\mathbf{g}}_k$ are corrupted. We thus apply error-control codes to encode the device index information to vector $\tilde{\mathbf{g}}_k$ with $C_1 = \lceil \log N \rceil / R$ OFDM symbols, where R is the code rate. For the third segment, we let the entries of $\dot{\mathbf{g}}_k$ be generated according to i.i.d. Rademacher (± 1) variables. The intuition of using the random Rademacher sequence is to assign a unique signature to different devices such that any false alarm can be identified. The number of symbols C_0, C_1 and C_2 will be specified later.

For device k , we let $|\mathcal{B}_k| = T$ and the set of bins are taken independently uniformly at random from the set $\{0, \dots, B-1\}$. Performing DFT on the OFDM symbols results in hashing of every device to T out of B bins uniformly at random. Fig. 4 illustrates an example for the case of $T = 2$. The reason of transmitting at T different frequency bins is to resolve the bin collision issue. The intuition is that, with a sufficiently large T , a sufficient number of devices are hashed to a singleton bin at least once with high probability.

Signaling for timing synchronization: The synchronization subframe consists of C_3 OFDM symbols, which are used to estimate of the delay of each device. Each symbol consists of B samples. For each OFDM symbol, we assign pseudonoise sequences on the frequencies such that the time-domain samples are Gaussian distributed. The synchronization can be achieved by performing the correlation between the received signal and the pilot symbols.

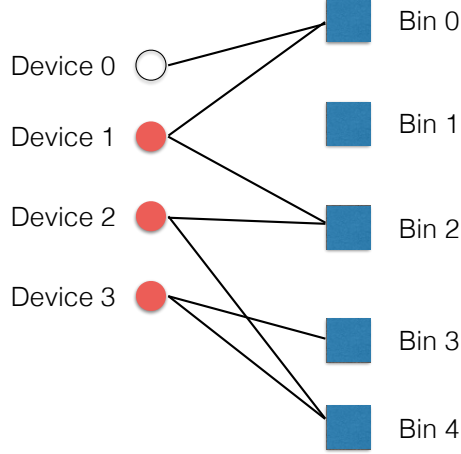


Fig. 4: Bipartite graph representation of sparse OFDM with $T = 2$.

IV. ASYNCHRONOUS NEIGHBOR DISCOVERY ALGORITHM

We first describe a robust bin detection that achieves two goals: (i) It can distinguish whether a frequency bin is a zero-ton, a singleton, or a multiton bin, as defined in Section III-B; (ii) For singleton bins, it can detect the device index reliably. Then we describe the overall asynchronous neighbor discovery scheme.

A. Robust Bin Detection

We focus on a certain device k that is hashed to bin b . The frequency value is given by $\mathbf{Y}_b = [\bar{\mathbf{Y}}_b^\dagger, \tilde{\mathbf{Y}}_b^\dagger, \dot{\mathbf{Y}}_b^\dagger]^\dagger$.

1) *Channel Phase Estimation:* Suppose the channel coefficient $A_{k,b}$ is known. We can make use of $\tilde{\mathbf{g}}_k$ to infer the device index. How to embed the device index information under the noiseless case has been described in Section III-B. In the noisy case, we use the first C_0 symbols to estimate the phase of $A_{k,b}$ as

$$\hat{\theta} = \angle \left(\frac{1}{C_0} \sum_{c=0}^{C_0-1} \bar{Y}_b^c \right). \quad (12)$$

Suppose device k transmits at a singleton frequency bin and C_0 is large enough, we can obtain an accurate estimate of the channel phase.

2) *Device Index Estimation:* With the phase estimation $\hat{\theta}_k$, we can compensate the phase of $A_{k,b}$ and try to decode the device index information. It can be seen that for singleton bins, the random transformation $\tilde{g}_k^c \rightarrow \text{Re} \left\{ \tilde{Y}_b^c e^{-i\hat{\theta}_k} \right\}$ is equivalent to a binary-input additive white Gaussian noise (BI-AWGN) channel.

In order to robustly estimate the information bits $(k_0, \dots, k_{\lceil \log N \rceil - 1})$, which is the binary representation of the device index k , we apply error control codes to code over the bits. Instead of transmitting $\lceil \log N \rceil$ OFDM symbols, we transmit $C_1 = \lceil \log N \rceil / R$ symbols, where the symbols carry the coded bits with code rate R . In particular, we construct $C_1 = \lceil \log N \rceil / R$ OFDM symbols with $\tilde{g}_k^c = (-1)^{r_{k,c}}$, $c = 0 \dots, C_1 - 1$, and

$$[r_{k,0}, \dots, r_{k,C_1-1}] = [k_0, \dots, k_{\lceil \log N \rceil - 1}] \mathbf{G}, \quad (13)$$

where the operation is over the binary field and $\mathbf{G} \in \mathbb{F}_2^{\lceil \log N \rceil \times C_1}$ is a generator matrix of an error-control code with rate R . We can apply the low-complexity capacity approaching codes [34]. For each bin b , we perform hard decoding on $\text{Re} \left\{ \tilde{\mathbf{Y}}_b^c e^{-j\hat{\theta}_k} \right\}$ for each symbol c , decode the sequence and then obtain the estimated index information. We focus on index estimation for singleton bins, because it allows us to apply the well-studied point-to-point capacity approaching codes. A more sophisticated soft decoding method can also be used. In this paper, we show that even a simple hard decoding is sufficient to guarantee reliable index estimation.

3) *Singleton Verification*: We can perform device index estimation for every frequency bin. Suppose a bin is singleton, the device that is hashed to it can be reliably detected. However, it may produce false alarms for multiton and zero-ton bins. We need to provide a mechanism to verify if the estimated index comes from a singleton bin. We refer to this process as singleton verification.

We generate C_2 symbols with \dot{g}_k^c being i.i.d. Rademacher variables, i.e., $P\{\dot{g}_k^c = \pm 1\} = 1/2$. Consider the analysis on a fixed bin b . First, we claim bin b is a zero-ton if the energy of $\dot{\mathbf{Y}}_b$ is low enough. Suppose \hat{k} is the estimated index from bin b . We perform the following validation process. We estimate the nonzero signal as

$$\dot{A}_{\hat{k},b} = \frac{1}{C_2} \dot{\mathbf{g}}_{\hat{k}}^\dagger \dot{\mathbf{Y}}_b. \quad (14)$$

Then we claim that \hat{k} is a correct estimate only if it passes the energy threshold test, i.e.,

$$\|\dot{\mathbf{Y}}_b - \dot{A}_{\hat{k},b} \dot{\mathbf{g}}_{\hat{k}}\|_2^2 \leq \eta. \quad (15)$$

The above validation scheme is similar to that used for sparse DFT and sparse WHT, where the singleton verification approach proved to work for signal amplitudes lying in a known discrete alphabet [29], [35]. In this paper, we further show that it can effectively identify the singletons for *arbitrary* signal amplitudes that are bounded away from zero.

4) *Overall Bin Detection*: Putting together, the robust bin detection algorithm is illustrated in Algorithm 1. For each frequency bin b , the DFT values is decomposed into three segments $\mathbf{Y}_b = [\bar{\mathbf{Y}}_b, \tilde{\mathbf{Y}}_b, \dot{\mathbf{Y}}_b]$. We declare the bin as a zero-ton if $\|\dot{\mathbf{Y}}_b\|^2 < \eta$, there η is some constant threshold. If the frequency bin is not a zero-ton, it is either a singleton or a multiton. We first estimate the phase of channel coefficient based on $\bar{\mathbf{Y}}_b$, compensate the phase for $\tilde{\mathbf{Y}}_b$ and estimate the device index as \hat{k} . The channel coefficient is estimated as $\dot{A}_{\hat{k},b}$ according to (14). If (15) is satisfied, a singleton is declared and the device \hat{k} is estimated to be active. Otherwise, a multiton bin is declared.

B. Overall Framework

Based on the previous description of robust bin detection, the active device can be reliably estimated whenever it is hashed to a singleton frequency bin regardless of the delay. Once a device index is estimated, its contribution to the connected bins can be canceled out, which may result in more singleton bins. For example, in Fig. 4, device 1 is first detected from the singleton bin 0 and its values are subtracted from bin 2. Then bin 2 becomes a singleton bin and device 2 can be detected from it. There is, however, one challenge. The DFT values from each device at a bin depends on its delay due to (6). We need to estimate the delay in order to perform successive cancellation. The second subframe is used for this purpose.

Algorithm 1 Robust-Bin-Detect (\mathbf{Y})

Input: Bin values $\mathbf{Y} = [\bar{\mathbf{Y}}, \tilde{\mathbf{Y}}, \dot{\mathbf{Y}}]$, where $\bar{\mathbf{Y}} \in \mathbb{C}^{C_0}$, $\tilde{\mathbf{Y}} \in \mathbb{C}^{C_1}$ and $\dot{\mathbf{Y}} \in \mathbb{C}^{C_2}$.

Output: Estimated active device index i .

if $\|\dot{\mathbf{Y}}\|^2 < \eta$ **then**

 Declare zero-ton and return $i \leftarrow \emptyset$.

end if

Phase estimation: $\hat{\theta} \leftarrow \text{phase}(\mathbf{1}^T \bar{\mathbf{Y}} / C_0)$.

Index location: $\mathbf{Z} \leftarrow \text{Re}\{\tilde{\mathbf{Y}} e^{-j\hat{\theta}}\}$,

$\hat{k} \leftarrow \text{Decoder}(\mathbf{Z})$.

Singleton verification:

$\hat{\mathbf{A}}_{\hat{k}} \leftarrow \hat{\mathbf{g}}_{\hat{k}}^\dagger \dot{\mathbf{Y}} / C_2$.

if $\|\dot{\mathbf{Y}} - \hat{\mathbf{A}}_{\hat{k}} \hat{\mathbf{g}}_{\hat{k}}\|_2^2 \leq \eta$ **then**

 Declare a singleton and return $i \leftarrow \hat{k}$.

else

 Declare a multi-ton and return $i \leftarrow \emptyset$.

end if

Algorithm 2 Asynchronous Neighbor Discovery via Sparse OFDM

Output: Detected active devices $\hat{\mathcal{K}}$.

Initialize: Set \mathcal{B} as the set of unprocessed bins. Set $\mathcal{L} = \emptyset$.

Global singleton estimation:

for $b \in \mathcal{B}$ **do**

$\hat{k} \leftarrow \text{Robust-Bin-Detect}(\bar{\mathbf{Y}}_b, \tilde{\mathbf{Y}}_b, \dot{\mathbf{Y}}_b)$.

if $\hat{k} \neq \emptyset$ **then**

$\hat{\mathcal{K}} \leftarrow \hat{\mathcal{K}} \cup \{\hat{k}\}$

$\mathcal{L} \leftarrow \mathcal{L} \cup \{\hat{k}\}$.

$\mathcal{B} \leftarrow \mathcal{B} \setminus b$.

 Estimate $\hat{m}_{\hat{k}}$ and $\hat{a}_{\hat{k}}$ according to (18) and (19).

end if

end for

Successive cancellation:

for $k \in \mathcal{L}$ **do**

$\mathcal{L} \leftarrow \mathcal{L} \setminus k$.

for Every bin $b \in \mathcal{B}$ that is connected with k **do**

$\bar{\mathbf{Y}}_b \leftarrow \bar{\mathbf{Y}}_b - \hat{a}_k \exp\left(\frac{j2\pi b(M - \hat{m}_k)}{B}\right) \mathbf{1}$.

$\tilde{\mathbf{Y}}_b \leftarrow \tilde{\mathbf{Y}}_b - \hat{a}_k \exp\left(\frac{j2\pi b(M - \hat{m}_k)}{B}\right) \tilde{\mathbf{g}}_k$.

$\dot{\mathbf{Y}}_b \leftarrow \dot{\mathbf{Y}}_b - \hat{a}_k \exp\left(\frac{j2\pi b(M - \hat{m}_k)}{B}\right) \dot{\mathbf{g}}_k$.

$\hat{k} \leftarrow \text{Robust-Bin-Detect}(\bar{\mathbf{Y}}_b, \tilde{\mathbf{Y}}_b, \dot{\mathbf{Y}}_b)$.

if $\hat{k} \neq \emptyset$ **then**

$\hat{\mathcal{K}} \leftarrow \hat{\mathcal{K}} \cup \{\hat{k}\}$

$\mathcal{L} \leftarrow \mathcal{L} \cup \{\hat{k}\}$.

$\mathcal{B} \leftarrow \mathcal{B} \setminus b$.

end if

end for

end for

Denote the set of BC_3 samples in the synchronization subframe as

$$\mathcal{I} = \{(B + M)CT, (B + M)CT + 1, \dots, (B + M)CT + BC_3 - 1\}. \quad (16)$$

Define the decision statistic as

$$\mathcal{T}(m) = \sum_{i \in \mathcal{I}} y_{i+m} s_{k,i}^*. \quad (17)$$

Assume no noise and correct delay estimate, $\mathcal{T}(m) = |a_k|^2 BC_3$. We estimate the delay of device k as

$$\hat{m}_k = \arg \max_{m=0, \dots, M} |\mathcal{T}(m)|. \quad (18)$$

Given an estimate of delay \hat{m}_k , the channel coefficient is estimated to be

$$\hat{a}_k = \frac{1}{C} \mathbf{g}_k^\dagger \mathbf{Y}_b e^{-\frac{j2\pi b(M - \hat{m}_k)}{B}}. \quad (19)$$

The DFT values of a connected unprocessed bin b' are then updated according to

$$\mathbf{Y}_{b'} \leftarrow \mathbf{Y}_{b'} - \hat{a}_k \exp\left(\frac{j2\pi b'(M - \hat{m}_k)}{B}\right) \mathbf{g}_k. \quad (20)$$

The robust bin detection algorithm is further performed on each updated frequency bin.

The overall device identification framework is described in Algorithm 2. Throughout the algorithm, we maintain three lists: $\hat{\mathcal{K}}$ is a list storing the estimated device indices, \mathcal{L} is a list of devices that are to be successively cancelled out from the bipartite graph, and \mathcal{B} is a list of unprocessed frequency bins. At the start of the algorithm, we initialize the lists $\hat{\mathcal{K}}$ and \mathcal{L} as empty, and \mathcal{B} as the set of all frequency bins. We first perform singleton estimation on all frequency bins. For each bin identified as a singleton, we remove it from \mathcal{B} and add its corresponding device index estimate \hat{k} to the lists of \mathcal{L} and $\hat{\mathcal{K}}$. Then we perform successive cancellation as follows: for each device index $k \in \mathcal{L}$, subtract its contribution to all connected bins as (20). Algorithm 1 is then performed on each connected bin. For every bin identified as a singleton, we remove it from \mathcal{B} and add its corresponding device index estimate to the list \mathcal{L} and $\hat{\mathcal{K}}$. This process continues until \mathcal{L} is empty.

We have presented the overall framework for device identification. In the following, we will prove by analysis that sparse OFDM can efficiently identify the active devices. We will first prove the synchronous case, i.e., $M = 0$, in Section V and extend the proof to the asynchronous case in Section VI.

V. PROOF OF THEOREM 1 (THE SYNCHRONOUS CASE)

We prove Theorem 1 in the asymptotic regime as K increases without bound. Here is an outline of the proof using $O(\cdot)$ notation¹ and a rigorous proof is provided afterwards. We choose some $B = O(K)$ and $T = O(1)$. In the codeword structure, the number of symbols is chosen as $C_0 = C_1 = C_2 = O(\log N)$. Due to synchronicity, there is no need to estimate the delays, so we set $C_3 = 0$. The total code length is $L = BC = O(K \log N)$. We need

¹For the $O(\cdot)$ notation, we assume that the number of active devices K and the maximum delay M scale in terms of N .

to perform B -point DFT for $C = O(\log N)$ symbols. The total computational complexity is $O(K(\log K)(\log N))$ using FFT operations. For each bin, the index estimation involves $O(\log N)$ operations and the phase estimation involves $O(\log N)$ operations. Since there are $O(K)$ bins, the total complexity due to phase estimation and index estimation is $O(K \log N)$. The total computational complexity is thus $O(K(\log K)(\log N))$.

Neighbor discovery is said to fail if there is any miss or false alarm. The analysis for the bin detection error probability follows exactly as in [36] if the channel coefficient is known or is constrained to lie in a finite alphabet. The key challenge here is that the channel coefficient is an arbitrary unknown value and the residual estimation error may propagate through the successive cancellation process. We will prove that neighbor discovery fails with probability $O(1/K)$ for some $T = O(1)$, $B = O(\log K)$ and $C = O(\log N)$. Specifically, the parameters are chosen as

$$T \geq 3 \quad (21)$$

$$B = \beta_0 K \quad (22)$$

$$C_0 = \lceil \log N \rceil \quad (23)$$

$$C_1 = \lceil \log N \rceil / R \quad (24)$$

$$C_2 = \beta_1 \lceil \log N \rceil, \quad (25)$$

where $\beta_0 \geq 2T(T-1)$, R is the code rate of a low-complexity binary-symmetric channel (BSC) capacity-approaching codes such that the transmission of $\lceil \log N \rceil$ bits under an SNR of $\underline{a}^2/(32\sigma^2/B)$ succeeds with probability higher than $1 - 1/N^2$ [34], and β_1 is some constant that will be specified later (Theorem 4). Given the parameter setting, the total number of OFDM symbols is $C = (1 + \beta_1 + 1/R)\lceil \log N \rceil$.

Let \mathcal{G} denote the ensemble of bipartite graphs that consist of only trees and components with a single cycle, and the largest component has fewer than $\beta_2 \log K$ left nodes, where β_2 is some constant depending on β_0 . Suppose the sparse OFDM induced bipartite graph G belongs to \mathcal{G} and the robust bin detection Algorithm 1 does not make any error, then the graph structure \mathcal{G} is sufficient to guarantee successful successive cancellation [37, Lemma 3.4], i.e., every active device index will be detected based on Algorithm 2. In the following, we will first show that $G \in \mathcal{G}$ with high probability (Claim 1). We then characterize the error propagation effects for the case of $G \in \mathcal{G}$ (Claim 2), and show that the robust bin detection succeeds with high probability (Claim 3). It follows immediately that synchronous neighbor discovery via Algorithm 2 succeeds with high probability.

Claim 1: Given the parameter setting (21)-(25), the sparse OFDM induced bipartite graph G satisfies $\mathbb{P}\{G \in \mathcal{G}\} \geq 1 - \gamma_0/K$, where γ_0 is some constant depending on β_0 .

Claim 2: Given $G \in \mathcal{G}$ and the parameter setting (21)-(25), the residual error of channel estimation are Gaussian variables with zero mean and variance bounded by $\beta_3 \sigma^2/B$, where $\beta_3 = 8\beta_2/(1 + \beta_1 + 1/R)$.

Claim 3: Given $G \in \mathcal{G}$ and the parameter setting (21)-(25), the robust bin detection Algorithm 1 fails to identify a zero-ton, a singleton, or a multiton with probability no greater than γ_1/K^2 for some γ_1 .

Let E_b denote the event that the robust bin detection Algorithm 1 makes an error throughout the process of Algorithm 2. Neighbor discovery succeeds if $G \in \mathcal{G}$ and E_b does not occur. Therefore, the error probability of

neighbor discovery is upper bounded as

$$P_s \leq P\{E_b|G \in \mathcal{G}\} + P\{G \notin \mathcal{G}\}. \quad (26)$$

Every time a device is recovered, Algorithm 1 is performed on its connected bins. Since there are K active devices and each of them is connected to $T = O(1)$ frequency bins, Algorithm 1 runs for at most KT times throughout the detection process. By the union bound and the result of Claim 3,

$$P\{E_b|G \in \mathcal{G}\} \leq \gamma_1 KT/K^2 = \gamma_1 T/K. \quad (27)$$

Combining Claim 1, (26) and (27), neighbor discovery fails with probability

$$P_s \leq (\gamma_0 + \gamma_1 T)/K. \quad (28)$$

Therefore, given the choice of T , B and C , neighbor discovery fails with probability less than ϵ for $K \geq (\gamma_0 + \gamma_1 T)/\epsilon$. The required code length is $BC = \beta_0(1 + \beta_1 + 1/R)K \lceil \log N \rceil$.

The proofs of Claim 2 and 3 will be given in the following sections.

A. Proof of Claim 1

A hypergraph is a generalization of a graph in which an edge can join any number of vertices. The sparse OFDM induced bipartite can be converted to a hypergraph where the device nodes represent the hyperedges and the frequency bins represent the vertices. The hyperedge is incident on a vertex if the corresponding device node is connected to the corresponding frequency bin. By the construction of the sparse OFDM, the induced hypergraph is a random T -uniform hypergraph, where every hyperedge has a degree T .

The well-established results on random hypergraph in [38] show that if B is chosen according to (22), the random T -uniform hypergraphs is composed entirely of hypertrees and unicyclic components with probability $1 - O(1/K)$. The intuition is that as B gets large, the random uniform hypergraph is composed of many small connected components with high probability. Moreover, the number of hyperedges in the largest connected component is $O(\log K)$ with probability $1 - O(1/K)$ [39]. Therefore, Claim 1 follows by the union bound.

B. Proof of Claim 2

We make use of the error propagation graph proposed in [33] to characterize the residual estimation error of channel estimation. For completeness, we describe the idea of error propagation graph in the following.

An error propagation graph for device k is a subgraph induced by the neighbor discovery Algorithm 2, which contains the device nodes that are recovered before device k , and have paths to device k in the bipartite graph. Fig. 5 illustrates the error propagation graph for device 2. In the error propagation graph, device 0 is estimated from singleton bin-a in the first iteration and its values are subtracted from the connected bins-b and c. In the second iteration, bin-b becomes a singleton bin. Device 1 can be detected and its values are subtracted from bin-c. In the third iteration, bin-c becomes a singleton bin and device 2 is detected.

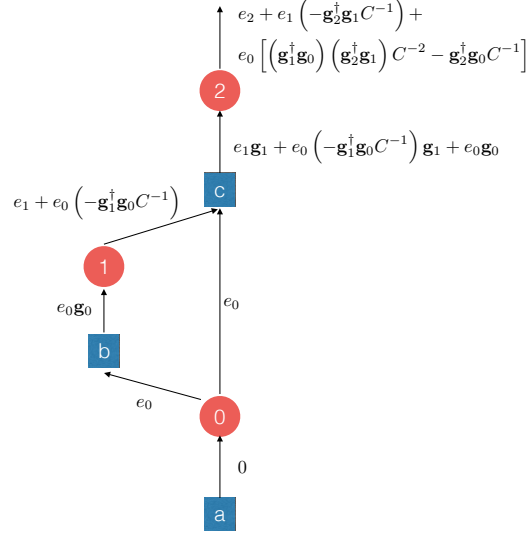


Fig. 5: Error propagation graph for device 2. Device 0 is detected from bin a at iteration $t = 1$, device 1 is detected from bin b at iteration $t = 2$, and device 2 is detected from bin c at iteration $t = 3$.

Define the channel estimation error of device k as

$$p_k = A_{k,b} - \hat{A}_{k,b}, \quad (29)$$

where $A_{k,b}$ is given by (6) and $\hat{A}_{k,b} = \mathbf{g}^\dagger \mathbf{Y}_b / C$ is the estimate according to (19) with $M = m = 0$. Let b_k be the frequency bin used to recover the device k . Define

$$e_k = -\frac{1}{C} \mathbf{g}_k^\dagger \mathbf{W}_{b_k}. \quad (30)$$

We will keep track of p_k using the error propagation graph. The estimation error can be calculated recursively according to some message passing rules over the graph. In particular, let p_k be the channel estimation error propagated out of device node k and \mathbf{q}_j be a length- C error vector propagated out of frequency bin j . The errors can be calculated according to the following rules:

$$p_k = e_k + \left(-C^{-1} \mathbf{g}_k^\dagger \mathbf{q}_{\text{in}(k)} \right) \quad (31)$$

$$\mathbf{q}_j = \sum_{k \in \text{in}(j)} p_k \mathbf{g}_k, \quad (32)$$

where $\text{in}(k)$ denotes the indices of the frequency bins (device nodes) incoming to device node (frequency bin) k . Since we use one singleton bin to decode the device index, the input message to device node k in the error propagation graph comes from one frequency bin, i.e., $|\text{in}(k)| = 1$ for any device node k .

Let $S(t)$ denote the device indices that are detected in the t -th iteration. We first show that (31) and (32) hold for any $k \in S(1) \cup S(2)$ and then show that they hold for any k by induction. Consider the estimation of $A_{k,b}$,

$k \in S(1)$. The DFT value of frequency bin b_k and the residual estimation error are given by

$$\mathbf{Y}_{b_k} = A_{k,b_k} \mathbf{g}_k + \mathbf{W}_{b_k} \quad (33)$$

$$p_k = e_k. \quad (34)$$

Consider the estimation for A_{k,b_k} , $k \in S(2)$. Let b_k be the frequency bin used to recover device index k . With the successive cancellation process, the updated DFT values of frequency bin and the estimation error become

$$\mathbf{Y}_{b_k} = A_{k,b_k} \mathbf{g}_k + \mathbf{W}_{b_k} + \sum_{\ell \in S(1): \ell \text{ connected with } b_k} e_\ell \mathbf{g}_\ell, \quad (35)$$

$$p_k = e_k + \sum_{\ell \in S(1): \ell \text{ connected with } b_k} e_\ell \left(-C^{-1} \mathbf{g}_k^\dagger \mathbf{g}_\ell \right) \quad (36)$$

$$= e_k + \left(-C^{-1} \mathbf{g}_k^\dagger \mathbf{q}_{b_k} \right), \quad (37)$$

where $\mathbf{q}_{b_k} = \sum_{\ell \in \text{in}(b_k)} e_\ell \mathbf{g}_\ell$. It is important to note that $|\mathbf{g}_k^\dagger \mathbf{g}_\ell C^{-1}| \leq 1$ for every realization of the design vectors.

Suppose the message passing rules (31) and (32) hold for $k \in S(t-1)$. For $k \in S(t)$, with successive cancellation, the updated frequency value is

$$\mathbf{Y}_{b_k} = A_{k,b_k} \mathbf{g}_k + \mathbf{W}_{b_k} + \sum_{\ell \in \text{in}(b_k)} p_\ell \mathbf{g}_\ell. \quad (38)$$

The channel estimation error is

$$p_k = A_{k,b_k} - \frac{1}{C} \mathbf{g}_k^\dagger \mathbf{Y}_{b_k} \quad (39)$$

$$= e_k - \sum_{\ell \in \text{in}(b_k)} C^{-1} p_\ell \mathbf{g}_k^\dagger \mathbf{g}_\ell \quad (40)$$

$$= e_k - C^{-1} \mathbf{g}_k^\dagger \mathbf{q}_{b_k}, \quad (41)$$

where (41) follows from the definition of \mathbf{q}_{b_k} . In the error propagation graph, $b_k = \text{in}(k)$ and the message passing rules are thus proved to hold for any k by induction.

By the error message passing rules (31) and (32), the estimation error of A_{k,b_k} , $k \in S(t)$, is calculated as

$$p_k = e_k + \sum_{\ell \in \cup_{j=1}^{t-1} S(j) \cap D(k)} \left(\sum_{p=1}^{\mathcal{P}(\ell,k)} d_{\ell,p} \right) e_\ell, \quad (42)$$

where $D(k)$ be the connected subgraph of the bipartite graph containing node k , $\mathcal{P}(\ell,k)$ is the number of paths from node ℓ to node k in $D(k)$, and $d_{\ell,p}$ is some coefficient depending on both the design parameters $\{\mathbf{g}_k\}$ and the path, which satisfies $|d_{\ell,p}| \leq 1$.

Fig. 5 illustrates an example. The number of paths from node 0 to node 2 is $\mathcal{P}(0,2) = 2$, with the corresponding coefficients being $d_{0,1} = -\mathbf{g}_2^\dagger \mathbf{g}_0 / C$ and $d_{0,2} = \mathbf{g}_1^\dagger \mathbf{g}_0 \mathbf{g}_2^\dagger \mathbf{g}_1 / C^2$. The number of paths from node 1 to node 2 is $\mathcal{P}(1,2) = 1$, with the coefficients being $d_{1,1} = -\mathbf{g}_2^\dagger \mathbf{g}_1 / C$.

Suppose $G \in \mathcal{G}$, the frequency value for any singleton bin b_k for device k can be written as

$$\mathbf{Y}_{b_k} = A_{k,b_k} \mathbf{g}_k + \mathbf{W}_{b_k} + \mathbf{V}_{b_k}, \quad (43)$$

where \mathbf{V}_{b_k} is the interference on bin b_k due to the channel estimation residual errors. Mathematically, it can be calculated as

$$\mathbf{V}_{b_k} = \sum_{\ell \in \cup_{j=1}^{t-1} S(j) \cap D(k)} \sum_{p=1}^{P(\ell,k)} e_\ell d_{\ell,p} \mathbf{g}_{\ell_p}, \quad (44)$$

where $\ell_p \in \text{in}(b_k)$ depends on the path from ℓ to bin b_k . The error e_ℓ is given by (30). It is easy to see that every e_ℓ is independent of the design parameters $\{\mathbf{g}_k\}$ of all the devices and is distributed according to $\mathcal{CN}(0, 2\sigma^2/(BC))$.

Suppose the bipartite graph belongs to \mathcal{G} , $P(\ell, k)$ is less than or equal to 2. Moreover, by Claim 1, the number of left nodes in each component is less than $\beta_2 \log K$. Conditioned on the design parameters \mathbf{g}_ℓ of the previously identified devices, each entry of \mathbf{V}_{b_k} is Gaussian variable with zero mean and variance bounded by $8\beta_2 \log K \sigma^2 / (BC) \leq \beta_3 \sigma^2 / B$, where $\beta_3 = 8\beta_2 / (1 + \beta_1 + 1/R)$.

C. Proof of Claim 3

Let $E_{b,0}, E_{b,1}, E_{b,2}$ denote the failure of robust bin detection Algorithm 1 for a zero-ton, singleton and multiton, respectively. Suppose $G \in \mathcal{G}$, we will show that with a proper choice of the threshold η in Algorithm 2, the error probabilities can be bounded as $\mathbb{P}\{E_{b,i}\} = O(1/K^2)$, $i = 0, 1, 2$. Then the bin detection error is less than γ_1/K^2 for some γ_1 .

As described in the proof of Claim 2, the frequency values of a bin b can be written as

$$\mathbf{Y}_b = \sum_{k \in \mathcal{K}: b \in \mathcal{B}_k} A_{k,b} \mathbf{g}_k + \mathbf{W}_b + \mathbf{V}_b, \quad (45)$$

where the sum is over the set of active devices that are hashed to frequency bin b and not yet recovered, and \mathbf{V}_b is due to the residual channel estimation errors from the recovered devices. The detection error depends on \mathbf{V}_b and hence on the number of devices that cause interference. Let $\mathbf{Z}_b = \mathbf{W}_b + \mathbf{V}_b$ denote the interference plus noise. We set the energy thresholds as

$$\eta = C_2 \tau_0 / \sqrt{B} \quad (46)$$

where τ_0 is some constant that will be specified later.

1) *Zero-ton Error Detection:* For a zero-ton bin b , the DFT values are composed of purely noise and interference, i.e., $\mathbf{Y}_b = \mathbf{Z}_b$. The zero-ton error $E_{b,0}$ occurs only if $\|\dot{\mathbf{Y}}_b\|$ is greater than the threshold η . Thus,

$$\mathbb{P}\{E_{b,0}\} = \mathbb{P}\left\{\|\dot{\mathbf{Z}}_b\|_2^2 \geq \eta\right\} \quad (47)$$

$$\leq C_2 \mathbb{P}\left\{|\dot{Z}_{b,c}|^2 \geq \frac{\eta}{C_2}\right\}. \quad (48)$$

Let \underline{g} denote the set of design parameters \mathbf{g}_k of all the previously identified devices. Conditioned on \underline{g} , each entry of \mathbf{Z}_b is distributed according to $\mathcal{CN}(0, 2\sigma_z^2)$, where $\sigma_z \leq (1 + \beta_3/2)\sigma^2/B$. The probability of passing the energy threshold is

$$\mathbb{P}\left\{|\dot{Z}_{b,c}|^2 \geq \frac{\eta}{C_2} | \underline{g}\right\} \leq 2\mathbb{P}\left\{|\operatorname{Re}\{\dot{Z}_{b,c}\}|^2 \geq \frac{\eta}{2C_2} | \underline{g}\right\} \quad (49)$$

$$\leq 4e^{-\frac{\eta}{4\sigma_z^2 C_2}} \quad (50)$$

$$\leq 4e^{-\frac{B\eta}{(4+2\beta_3)\sigma^2 C_2}}. \quad (51)$$

With B and C_2 chosen according to (22) and (25), respectively, there exists τ_0 such that $C_2 4e^{-\frac{B\eta}{(4+2\beta_3)\sigma^2 C_2}} \leq 1/K^2$.

Moreover, (51) holds for every realization of \underline{g} , by averaging \underline{g} , we have

$$\mathbb{P}\left\{\|\dot{\mathbf{Z}}_b\|_2^2 \geq \eta\right\} \leq C_2 \mathbb{P}\left\{|\dot{Z}_{b,c}|^2 \geq \frac{\eta}{C_2}\right\} \quad (52)$$

$$\leq \frac{1}{K^2}. \quad (53)$$

Combining (48) and (53), we have

$$\mathbb{P}\{E_{b,0}\} \leq \frac{1}{K^2}. \quad (54)$$

2) *Singleton Error Detection*: Suppose device k is hashed to a singleton bin b . Let $E_{b,1}$ denote the bin detection error. A singleton detection error occurs due to three events: (1) $E_{b,1,0} = \left\{\|\dot{\mathbf{Y}}_b\|_2^2 < \eta\right\}$; (2) $E_{b,1,1} = \left\{\|\dot{\mathbf{Y}}_b - \dot{A}_{k,b}\dot{\mathbf{g}}_k\|_2^2 > \eta\right\}$; (3) $E_{b,1,2} = \left\{\hat{k}_b \neq k\right\}$. Thus $E_{b,1} \subseteq E_{b,1,0} \cup E_{b,1,1} \cup E_{b,1,2}$.

By large deviation, with high probability $\|\dot{\mathbf{Y}}_b\|^2$ is concentrated around $C_2(|a_k|^2 + 2\sigma_z^2)$. Since $\eta = C_2\tau_0/\sqrt{B}$ and τ_0 is some fixed constant, $\|\dot{\mathbf{Y}}_b\|^2$ is greater than η for large enough K . In particular, it is proved in Appendix A that

$$\mathbb{P}\{E_{b,1,0}\} \leq \frac{2}{K^2}. \quad (55)$$

We next upper bound the probability of $E_{b,1,1}$. Let $\dot{A}_{k,b} = \dot{\mathbf{g}}_k^\dagger \dot{\mathbf{Y}}_b / C_2$. We have

$$\dot{\mathbf{Y}}_b - \dot{A}_{k,b}\dot{\mathbf{g}}_k = \left(\mathbf{I} - \frac{1}{C_2}\dot{\mathbf{g}}_k\dot{\mathbf{g}}_k^\dagger\right)\dot{\mathbf{Z}}_b. \quad (56)$$

Let $\mathbf{Q} = \mathbf{I} - \frac{1}{C_2}\dot{\mathbf{g}}_k\dot{\mathbf{g}}_k^\dagger$. Since $\dot{\mathbf{g}}_k^\dagger\dot{\mathbf{g}}_k = C_2$, $\dot{\mathbf{g}}_k$ is the eigenvector of $\dot{\mathbf{g}}_k\dot{\mathbf{g}}_k^\dagger/C_2$. Since $\dot{\mathbf{g}}_k\dot{\mathbf{g}}_k^\dagger/C_2$ is a rank-1 matrix, it has only a single nonzero eigenvalue which is 1. Therefore, the eigenvalue decomposition of \mathbf{Q} can be written as

$$\mathbf{Q} = \mathbf{U}\mathbf{\Lambda}\mathbf{U}^\dagger \quad (57)$$

$$= \mathbf{U}\operatorname{diag}\{0, 1, \dots, 1\}\mathbf{U}^\dagger \quad (58)$$

where \mathbf{U} is an orthogonal matrix. Then we have

$$\|\dot{\mathbf{Y}}_b - \dot{A}_{k,b}\dot{\mathbf{g}}_k\|_2^2 = \|\mathbf{Q}\dot{\mathbf{Z}}_b\|_2^2 \quad (59)$$

$$= \|\Lambda \mathbf{U}^\dagger \dot{\mathbf{Z}}_b\|_2^2 \quad (60)$$

$$= \sum_{c=1}^{C_2-1} |Z'_c|^2, \quad (61)$$

where $\mathbf{Z}' = \mathbf{U}^\dagger \dot{\mathbf{Z}}_b$ and (61) is due to $\Lambda = \text{diag}(0, 1, \dots, 1)$. Since $\|\dot{\mathbf{Z}}_b\|_2^2 = \|\mathbf{Z}'\|_2^2$, we have

$$\mathbf{P} \left\{ \|\dot{\mathbf{Y}}_b - \dot{A}_{k,b}\dot{\mathbf{g}}_k\|_2^2 \geq \eta \right\} = \mathbf{P} \left\{ \sum_{c=1}^{C_2-1} |Z'_c|^2 \geq \eta \right\} \quad (62)$$

$$\leq \mathbf{P} \left\{ \|\dot{\mathbf{Z}}_b\|_2^2 \geq \eta \right\} \quad (63)$$

$$\leq \frac{1}{K^2}, \quad (64)$$

where (64) follows from (53). Therefore, we have

$$\mathbf{P} \{E_{b,1,1}\} \leq \frac{1}{K^2}. \quad (65)$$

We next bound the error probability of $E_{b,1,2}$. We first show that the phase compensation is accurate with high probability. Second, we show that the interference only causes a slight SNR degradation with high probability. Third, the device index recovery can be regarded as transmission over a BSC channel and a large enough C_1 can help recover the index information.

We estimate the phase of $\theta = \angle A_{k,b}$ according to (12). Then the estimated phase is calculated as

$$\hat{\theta} = \angle (A_{k,b} + \bar{Z}), \quad (66)$$

where $\bar{Z} = \sum_{c=0}^{C_0-1} (\bar{W}_b^c + \bar{V}_b^c) / C_0$. From the geometric interpretation, the maximum phase offsets occurs when the noise is orthogonal to the measurement. We choose a small θ_0 such that $\theta_0 < \frac{\pi}{3}$ and $\sin \theta_0 > \theta_0/2$, then

$$\mathbf{P} \left\{ |\hat{\theta} - \theta| > \theta_0 \right\} \leq \mathbf{P} \left\{ \arcsin \frac{|\bar{Z}|}{|A_{k,b}|} > \theta_0 \right\} \quad (67)$$

$$\leq \mathbf{P} \left\{ |\bar{Z}| > \underline{a} \sin \theta_0 \right\} \quad (68)$$

$$\leq \mathbf{P} \left\{ |\bar{Z}| > \frac{a\theta_0}{2} \right\} \quad (69)$$

$$\leq \mathbf{P} \left\{ |\text{Re}\{Z\}| > \frac{a\theta_0}{4} \right\} + \mathbf{P} \left\{ |\text{Im}\{Z\}| > \frac{a\theta_0}{4} \right\} \quad (70)$$

$$\leq 4 \exp \left(-\frac{a^2 \theta_0^2}{32 \sigma_z^2} \right), \quad (71)$$

where (71) is due to $\mathbf{P}\{\mathcal{N}(0, 1) > x\} \leq e^{-x^2/2}$.

Therefore, given $B = \beta_0 K$, with high probability $1 - e^{-\Omega(K)}$,

$$\text{Re} \left\{ A_{k,b} e^{-i\hat{\theta}} \right\} = \underline{a} \cos(\hat{\theta} - \theta) \quad (72)$$

$$\geq \underline{a} \cos \theta_0 \quad (73)$$

$$\geq \underline{a}/2. \quad (74)$$

We consider the corruption of signal strength from interference \mathbf{V} . Since \tilde{V}_b^c is Gaussian distributed with variance less than or equal to $\beta_3 \sigma^2 / B$, $\text{P} \left\{ |\text{Re} \{ \tilde{V}_b^c \}| \geq \underline{a}/4 \right\} \leq e^{-\Omega(K)}$. Combining (74), we have $\text{Re} \left\{ A_{k,b} e^{-i\hat{\theta}} \tilde{g}_k^c + \tilde{V}_b^c \right\} = c \tilde{g}_k^c$ with $c \geq \underline{a}/4$ for all $c = 0, \dots, C_1 - 1$ with probability higher than $1 - C_1 e^{-\Omega(K)}$. Conditioned on this, the device index transmission corrupted by noise \mathbf{W}_b can be regarded as transmission over BSC channel with SNR being at least $(\underline{a}/4)^2 / (2\sigma^2 / B) = \underline{a}^2 / (32\sigma^2 / B)$. Since the error-control code with rate R used to encode the device index information $(k_0, \dots, k_{\lceil \log N \rceil - 1})$ is chosen such that the index can be recovered correctly with probability at least $1 - 1/N^2$, the singleton error occurs with probability

$$\text{P} \{ E_{b,1,2} \} \leq \frac{1}{N^2}. \quad (75)$$

By (55), (65) and (75), we conclude

$$\text{P} \{ E_{b,1} \} \leq \frac{4}{K^2}. \quad (76)$$

3) *Multiton Error Detection:* It is proved in Appendix B that

$$\text{P} \{ E_{b,2} \} \leq \frac{2}{K^2}. \quad (77)$$

Therefore, combining (54), (76) and (77), we conclude that the robust bin detection correctly identify the zero-ton, singleton or multiton with probability higher than $1 - 7/K^2$.

VI. PROOF OF THEOREM 2 (THE ASYNCHRONOUS CASE)

In the asynchronous neighbor discovery case, we choose the parameters according to (21)–(25). The number of OFDM symbols used for synchronization is $C_3 = \beta_4 \lceil \log(K + M) \rceil$, where β_4 is specified in Appendix C. In the codeword structure, the number of symbols is $C = O(\log N)$. The total code length in transmit symbols is thus

$$L = (B + M)C + BC_3 \quad (78)$$

$$= O((K + M) \log N + K \log(K + M)). \quad (79)$$

The FFT operation and channel estimation involve the same number of operations as the synchronous. Different from the synchronous, each device needs to estimate its delay once. The complexity of delay estimation is $MBC_3 = O(MK \log(K + M))$ (corresponding to M times auto-correlations). A total of K devices need to estimate their delays. The total computational complexity is thus $O(K(\log K)(\log N)) + O(K^2 M \log(K + M))$.

The following lemma shows that for each device the delay estimate is correct with high probability.

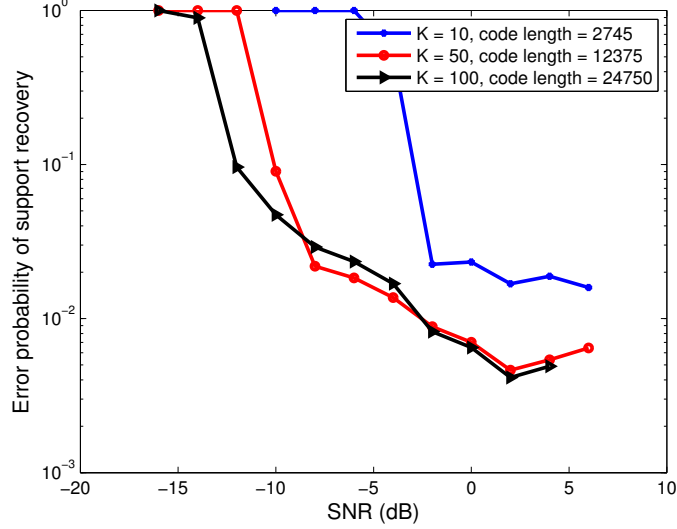


Fig. 6: Error probability of neighbor discovery in the case of synchronous transmission. The device population is $N = 2^{38}$.

Lemma 1: Suppose the conditions specified in Theorem 2 hold. Suppose the bipartite graph $G \in \mathcal{G}$ and the parameters are chosen according to (21)–(25), there exists some positive β_4 such that $C_3 = \beta_4 \lceil \log(K + M) \rceil$ OFDM symbols are used for timing synchronization and the delay of a device estimated according to (18) is correct with probability $O(1/K^2)$.

Proof See Appendix C.

By the union bound and Lemma 1, the delay of each device can be correctly estimated with probability $1 - O(1/K)$. Conditioned on that the device delays are correctly detected, the residual errors of channel estimation can be characterized in the same manner as the synchronous case. The proof for correct asynchronous neighbor discovery follows that for synchronous case.

VII. SIMULATION RESULTS

Throughout the simulation, we will present the error probability achieved by sparse OFDM for a network involving a massive number of devices. Specifically, the total number of devices is $N = 2^{38}$. The performance of sparse OFDM will be compared with two random access schemes, namely slotted ALOHA and CSMA. The goal of the simulation is to show that sparse OFDM is a viable design for massive communications, e.g., the IoT, thanks to the short code length and low computational complexity,

A. Synchronous neighbor discovery

We simulate the error probability of synchronous neighbor discovery via sparse OFDM. The number of bins assigned to each device is $T = 3$. The number of measurement bins is $B = \lceil 4.5K \rceil$, where K is the number of

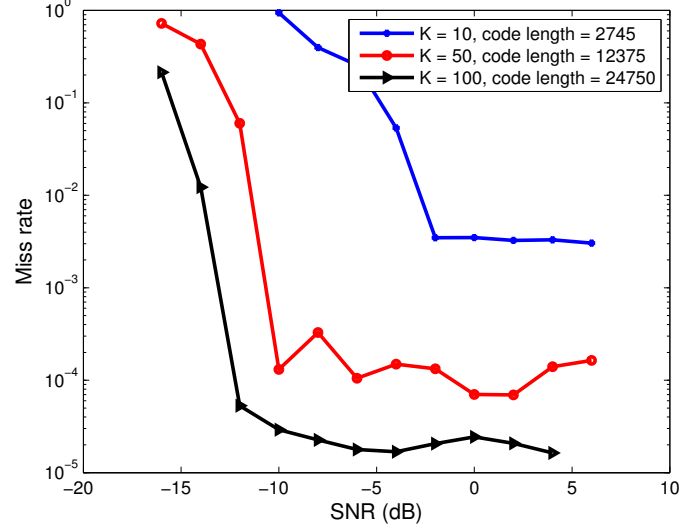


Fig. 7: Rate of missed detection in the case of synchronous transmission. The device population is $N = 2^{38}$.

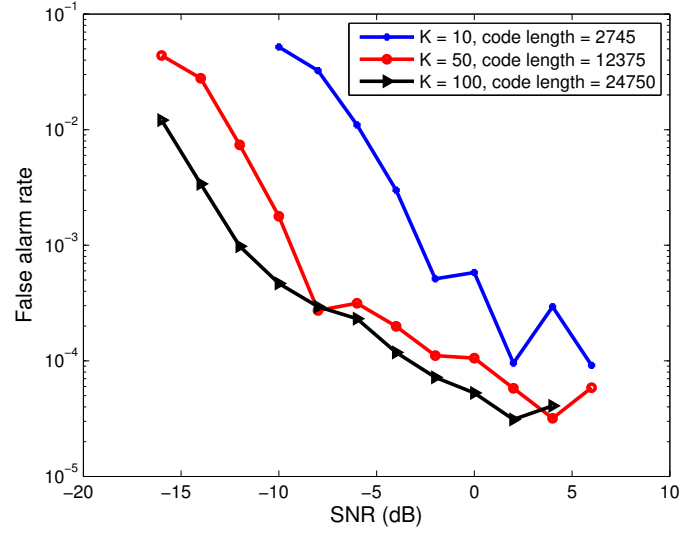


Fig. 8: Rate of false alarm in the case of synchronous transmission. The device population is $N = 2^{38}$.

active devices. The number of OFDM symbols for phase estimation singleton verification are set as $C_0 = 6$ and $C_2 = 6$, respectively. We adopt a rate $R = 0.9$ random LDPC code as subcode. The number of OFDM symbols carrying device index information is thus $C_1 = \lceil \log N \rceil / R$. The number of OFDM symbols used in synchronization is $C_3 = 8$.

Fig. 6 shows the error probability of device identification for asynchronous neighbor discovery. In each simulation, if there exists missed detection or false alarm, it claims to have an error. Fig. 7 and Fig. 8 show the miss and false alarm rates, respectively. We define the missed detection (false alarm) rate as the average number of misses (false alarms) in each simulation normalized by the number of active devices K . Simulation shows that under SNR of 6

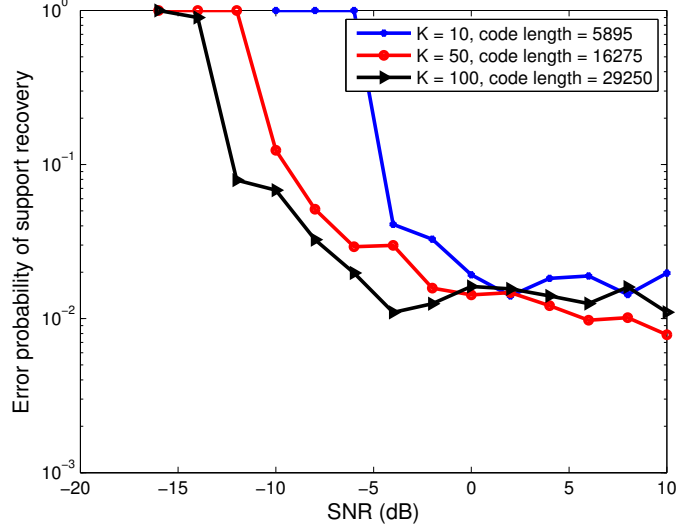


Fig. 9: Error probability of neighbor discovery in the case of discrete delay. The device population is $N = 2^{38}$ and the maximum delay is $M = 20$.

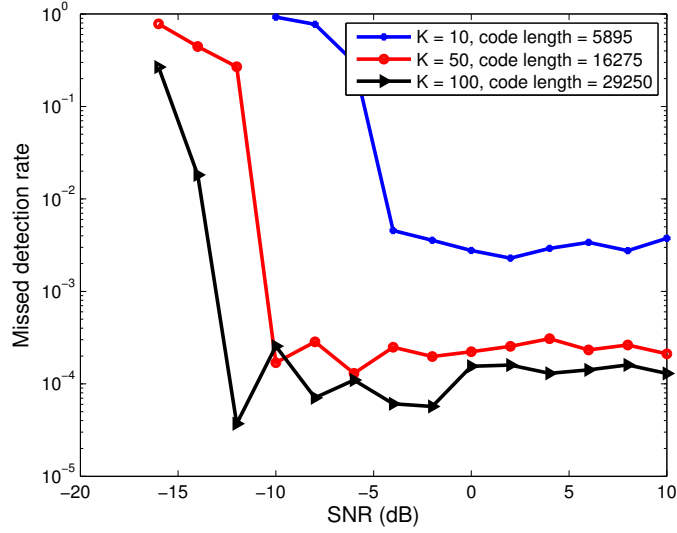


Fig. 10: Rate of missed detection in the case of discrete delay. The device population is $N = 2^{38}$ and the maximum delay is $M = 20$.

dB, in order to achieve miss detection and false alarm rate of 10^{-4} , the code length required to identify $K = 100$ out of 2^{38} devices is around 25000 samples. In the case of a 20 MHz channel bandwidth, the transmission time is approximately 1.25 ms. With a miss detection and false alarm rate of 10^{-4} , it implies that all the $K = 100$ active devices can be correctly estimated with high probability within a short time.

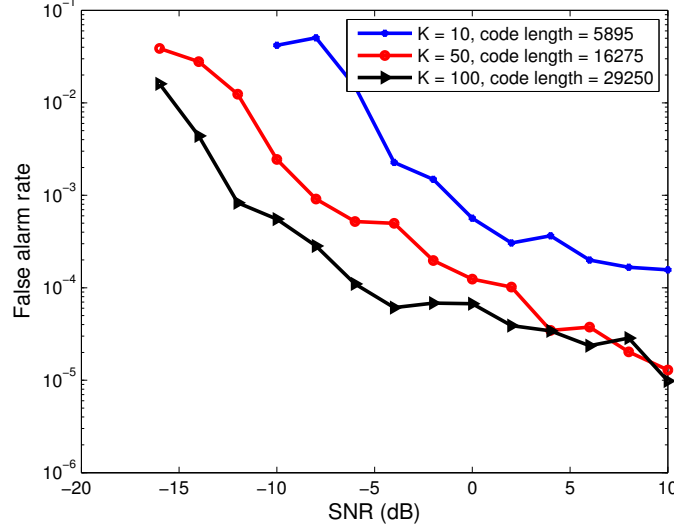


Fig. 11: Rate of false alarm in the case of discrete delay. The device population is $N = 2^{38}$ and the maximum delay is $M = 20$.

B. Asynchronous neighbor discovery

We simulate the error probability of asynchronous neighbor discovery via sparse OFDM. The system parameters are the same as in the synchronous setting. The device population is $N = 2^{38}$ and the maximum delay in terms of transmit samples is $M = 20$. The delay of each device transmission is assumed to be multiples of T_s . Fig. 9 shows the error probability of asynchronous neighbor discovery. Fig. 10 and Fig. 11 show the missed detection rate and false alarm rate, respectively. As in the synchronous setting, the error probability is low under moderate SNR, which confirms our theoretical analysis. In order to achieve a similar error performance, the required code length is more than that of synchronous setting.

C. Comparison with random access

1) *Slotted ALOHA*: First, consider slotted ALOHA, where every device transmits a frame with probability p independently in each slot over an N_s -slot period. The probability of one given neighbor being missed is equal to the probability that the device is unsuccessful in all N_s slots:

$$P_{\text{miss,aloha}} = (1 - (1 - p)^{K-1}p)^{N_s}. \quad (80)$$

Setting $p = 1/K$ minimizes $P_{\text{miss,aloha}}$.

2) *CSMA*: It is challenging, if not impossible, to implement CSMA-based wireless access. Due to the power asymmetry between devices and access points, a device may not be able to sense another device's transmission in the same cell. Suppose, nonetheless, devices can sense each other and CSMA is used. When the channel is idle, the devices start their timers. The device whose timer expires the first transmits. When the channel becomes busy, the

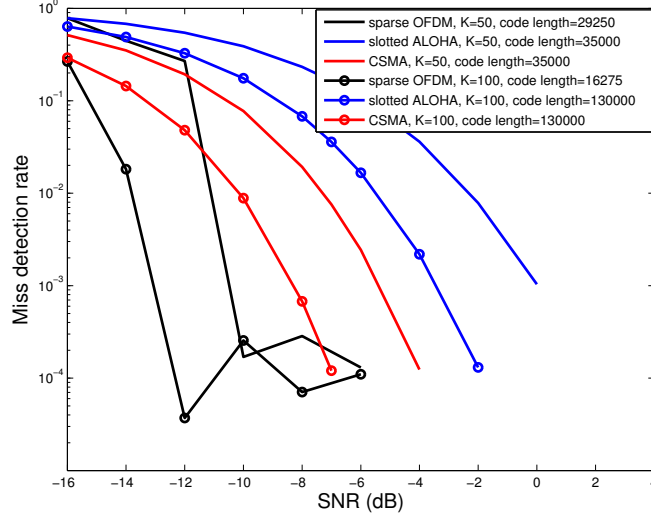


Fig. 12: Performance comparison between sparse OFDM and the random access schemes. The device population is $N = 2^{38}$ and the maximum delay is $M = 20$.

devices stop their timers. Device i has a chance to transmit if its timer is the minimum in some slot. The probability that a given device never gets a chance to transmit is

$$P_{\text{miss,csma}} = (1 - P\{T_1 < \min\{T_2, \dots, T_K\}\})^{N_s}. \quad (81)$$

In order to reliably transmit the device index $\log N$ bits, the number of symbols required in each frame is at least $\lceil \log N \rceil / \log(1 + \text{SNR})$. Therefore, the total number of symbols required is $N_s \lceil \log N \rceil / \log(1 + \text{SNR})$, where N_s depends on the target miss rate. Under $\text{SNR} = -4$ dB, it can be seen from Fig. 10 and Fig. 11 that sparse OFDM can achieve missed detection and false alarm rate low than 10^{-4} . The advantage of sparse OFDM over random access becomes more obvious as the number of active devices increases. Fig. 12 shows the performance comparison between sparse OFDM and random access schemes. When $K = 50$, the code length of sparse OFDM is around 16000, while slotted ALOHA and CSMA requires more than 35000 symbols to achieve a missed detection rate of 10^{-4} . Sparse OFDM can effectively reduce the code length by over 50%. Moreover, the code length reduction is even greater for larger K and a lower error probability requirement. When $K = 100$, $\text{SNR} = -7$ dB, and the target missed detection and false alarm rate is 10^{-4} , the code length of sparse OFDM needed is around 30000, while slotted ALOHA and CSMA requires more than 130000 symbols. Sparse OFDM can effectively reduce the code length by over 70%.

VIII. CONCLUSION

We have proposed a low-complexity asynchronous neighbor discovery scheme for very large networks with applications to the Internet of Things. The scheme, referred to as sparse OFDM, applies the recently developed sparse Fourier transform to compressed neighbor discovery. Compared with random access schemes, sparse OFDM

requires much shorter code length by exploiting the multiaccess nature of the channel and the multiuser detection gain. Sparse OFDM adopts well-established point-to-point capacity approaching codes and involves low complexity. It provides practical physical layer capability for multipacket reception and it would be a useful next step to extend this technique to the design of asynchronous neighbor discovery network protocols.

APPENDIX A

PROOF OF SINGLETON ERROR

We establish the following lemma to prove (55).

Lemma 2: Let B be given as (22). Let $0 \leq c < C_2$ and $\beta_3 \geq 0$ be some fixed constants. Let each entry of $\mathbf{Z} \in \mathbb{C}^{C_2}$ be distributed according to $\mathcal{CN}(0, 2\sigma_z^2)$, where $\sigma_z \leq (1 + \beta_3/2)\sigma^2/B$. Let $\mathbf{Q} = \mathbf{U}\mathbf{\Lambda}\mathbf{U}^\dagger$, where \mathbf{U} is a real-valued orthogonal matrix and $\mathbf{\Lambda} = \text{diag}\{0, \dots, 0, 1, \dots, 1\}$ is a diagonal matrix with c zeros and $C_2 - c$ ones. Let $\mathbf{S} = \sum_{k=1}^{k_0} A_{k,b} \mathbf{g}_k$, where $k_0 \geq 1$, the entries of \mathbf{g}_k are i.i.d. Rademacher variables, and $|A_{k,b}| \geq \underline{a}$. Then there exists some β_1 such that $C_2 = \beta_1 \lceil \log N \rceil$ and η is as defined in (46), the following holds for large enough K :

$$\mathbb{P} \left\{ \|\mathbf{Q}\mathbf{S} + \mathbf{Z}\|_2^2 \leq \eta \right\} \leq \frac{2}{K^2}. \quad (82)$$

Proof In the following, we write $\sum_{k=1}^{k_0}$ as \sum_k for succinct notation. We have

$$\begin{aligned} \mathbb{P} \left\{ \|\mathbf{Q}\mathbf{S} + \mathbf{Z}\|_2^2 \leq \eta \right\} &\leq \mathbb{P} \left\{ \|\mathbf{Q}\mathbf{S} + \mathbf{Z}\|_2^2 \leq \eta \mid \|\mathbf{Q}\mathbf{S}\|_2^2 \geq \frac{(C_2 - c) \sum_k |A_{k,b}|^2}{2} \right\} + \\ &\quad \mathbb{P} \left\{ \|\mathbf{Q}\mathbf{S}\|_2^2 \leq \frac{(C_2 - c) \sum_k |A_{k,b}|^2}{2} \right\}. \end{aligned} \quad (83)$$

Bounding the first item of (83): By the triangular inequality $\|\mathbf{Z}\|_2 + \|\mathbf{Q}\mathbf{S} + \mathbf{Z}\|_2 \geq \|\mathbf{Q}\mathbf{S}\|_2$, we have

$$\begin{aligned} &\mathbb{P} \left\{ \|\mathbf{Q}\mathbf{S} + \mathbf{Z}\|_2^2 \leq \eta \mid \|\mathbf{Q}\mathbf{S}\|_2^2 \geq \frac{(C_2 - c) \sum_k |A_{k,b}|^2}{2} \right\} \\ &\leq \mathbb{P} \left\{ \|\mathbf{Q}\mathbf{S}\|_2 - \|\mathbf{Z}\|_2 \leq \sqrt{\eta} \mid \|\mathbf{Q}\mathbf{S}\|_2^2 \geq \frac{(C_2 - c) \sum_k |A_{k,b}|^2}{2} \right\}. \end{aligned} \quad (84)$$

Since $\eta = C_2 \tau_0 / \sqrt{B}$, for B given by (22) and any fixed c, τ_0 , we have $\frac{(C_2 - c) \sum_k |A_{k,b}|^2}{2} \geq \frac{(C_2 - c) \underline{a}^2}{2}$, which is greater than 4η for large enough K . Therefore, for large enough K ,

$$\begin{aligned} &\mathbb{P} \left\{ \|\mathbf{Q}\mathbf{S}\|_2 - \|\mathbf{Z}\|_2 \leq \sqrt{\eta} \mid \|\mathbf{Q}\mathbf{S}\|_2^2 \geq \frac{(C_2 - c) \sum_k |A_{k,b}|^2}{2} \right\} \\ &\leq \mathbb{P} \left\{ \|\mathbf{Z}\|_2 \geq \sqrt{\eta} \mid \|\mathbf{Q}\mathbf{S}\|_2^2 \geq \frac{(C_2 - c) \sum_k |A_{k,b}|^2}{2} \right\} \end{aligned} \quad (85)$$

$$\leq 1/K^2, \quad (86)$$

where (86) is due to (64).

Bounding the second item of (83): We introduce the definition of subGaussian variable, which will be used in the proof.

Definition 1: X is σ -subGaussian if there exists $\sigma > 0$ such that

$$\mathbb{E} \left\{ \exp(tX) \right\} \leq \exp(\sigma^2 t^2 / 2), \quad \forall t \geq 0. \quad (87)$$

Definition 2 (subGaussian norm): The subGaussian norm of the random variable X is defined as

$$\|X\|_{\phi_2} = \sup_{p \geq 1} p^{-1/2} (\mathbb{E}|X|^p)^{1/p}. \quad (88)$$

The second item of (83) is derived in the following steps. We first show that the real and imaginary parts of \mathbf{S} are subGaussian variables. Then, we show that $\|\mathbf{Q}\mathbf{S}\|_2^2$ are concentrated around $(C_2 - c) \sum_k |A_{k,b}|^2$ with high probability using the large deviation results on subGaussian variables. In the following, we denote X_R and X_I as the real and imaginary component of X , respectively.

Lemma 3: Let $\mathbf{S}_R = (S_{0,R}, \dots, S_{C_2-1,R})$ and $\mathbf{S}_I = (S_{0,I}, \dots, S_{C_2-1,I})$ be the real and imaginary components of \mathbf{S} defined as (108), respectively. Then $S_{c,R}$ are i.i.d. $\sqrt{\sum_k A_{k,R}^2}$ -subGaussian random variables with $\mathbb{E}S_{c,R} = 0$ and the subGaussian norm satisfies $\|S_{c,R}\|_{\phi_2} \leq 2\sqrt{\sum_k A_{k,R}^2}$. Similarly, $S_{c,I}$ are i.i.d. $\sqrt{\sum_k A_{k,I}^2}$ -subGaussian random variables with $\mathbb{E}S_{c,I} = 0$ and the subGaussian norm satisfies $\|S_{c,I}\|_{\phi_2} \leq 2\sqrt{\sum_k A_{k,I}^2}$.

Proof Since \dot{g}_k^c is Rademacher variable, it is 1-subGaussian with mean zero. Thus, $\mathbb{E}S_{c,R} = 0$. Moreover, g_k^c are independent across k . According to Lemma 4 and Lemma 5, $S_{c,R} = \sum_k A_{k,R} \dot{g}_k^c$ is $\sqrt{\sum_k A_{k,R}^2}$ -subGaussian. $\{S_{c,R}\}_{c=0}^{C_2-1}$ are independent, because \dot{g}_k^c are independent across $c = 0, \dots, C_2 - 1$.

By Definition 1, $\mathbb{E}\{\exp(tS_{c,R})\} \leq \exp\left(\sum_k A_{k,R}^2 t^2/2\right)$. Let $X = S_{c,R}/\sqrt{2\sum_k A_{k,R}^2}$. Then $\mathbb{E}\{\exp(tX)\} \leq \exp(t^2/4)$. According to Theorem 3, for all $p \geq 1$, $(\mathbb{E}|X|^p)^{1/p} \leq \sqrt{2p}$, which yields

$$(\mathbb{E}|S_{c,R}|^p)^{1/p} \leq 2\sqrt{\sum_k A_{k,R}^2 p}. \quad (89)$$

By (88), the subGaussian norm of $S_{c,R}$ is upper bounded as $\|S_{c,R}\|_{\phi_2} \leq 2\sqrt{\sum_k A_{k,R}^2}$. The statement for the imaginary parts follow similarly.

In order to apply Theorem 4 to provide a concentration result on $\|\mathbf{Q}\mathbf{S}\|$, we need to first derive the Frobenius norm and the operator norm of \mathbf{Q} . The Frobenius norm of \mathbf{Q} is calculated as

$$\|\mathbf{Q}\|_F^2 = \text{tr}\{\mathbf{Q}\mathbf{Q}^\dagger\} \quad (90)$$

$$= \text{tr}\{\mathbf{Q}\} \quad (91)$$

$$= C_2 - c. \quad (92)$$

where (91) follows by $\mathbf{Q}\mathbf{Q}^\dagger = \mathbf{Q}$, and (92) follows because the sum of the eigenvalues of \mathbf{Q} is $C_2 - c$.

Since the largest eigenvalue of \mathbf{Q} is 1, the operator norm of \mathbf{Q} is calculated as

$$\|\mathbf{Q}\| = \max_{\mathbf{x} \neq 0} \frac{\|\mathbf{Q}\mathbf{x}\|_2}{\|\mathbf{x}\|_2} = 1. \quad (93)$$

Conditioned on \mathbf{g}_{k_0} ,

$$\mathbb{E} \{ \|\mathbf{Q}\mathbf{S}_R\|_2^2 \} = \mathbb{E} \{ \mathbf{S}_R^\dagger \mathbf{Q} \mathbf{Q}^\dagger \mathbf{S}_R \} \quad (94)$$

$$= \mathbb{E} \{ \mathbf{S}_R^\dagger \mathbf{Q} \mathbf{S}_R \} \quad (95)$$

$$= \mathbb{E} \{ S_{c,R}^2 \} \text{tr} \{ \mathbf{Q} \} \quad (96)$$

$$= (C_2 - c) \sum_k A_{k,R}^2, \quad (97)$$

where (96) follows because $\{S_{c,R}\}_{c=0}^{C_2-1}$ are i.i.d. distributed. Similarly, $\mathbb{E} \{ \|\mathbf{Q}\mathbf{S}_R\|_2^2 \} = (C_2 - c) \sum_k A_{k,I}^2$.

Applying Theorem 4 with $\mathbf{Z} = \mathbf{S}_R$, $\mathbf{A} = \mathbf{Q}$ with $\|\mathbf{Q}\| = 1$, $\|\mathbf{Q}\|_F^2 = C_2 - c$ and $K = 2\sqrt{\sum_k A_{k,R}^2}$ yields

$$\begin{aligned} & \mathbb{P} \left\{ \left| \|\mathbf{Q}\mathbf{S}_R\|_2^2 - (C_2 - c) \sum_k A_{k,R}^2 \right| > t \right\} \leq \\ & 2 \exp \left(-c_0 \min \left(\frac{t^2}{16(C_2 - c)(\sum_k A_{k,R}^2)^2}, \frac{t}{4 \sum_k A_{k,R}^2} \right) \right). \end{aligned} \quad (98)$$

Letting $t = (C_2 - c) \sum_k A_{k,R}^2 / 2$, we have

$$\mathbb{P} \left\{ \|\mathbf{Q}\mathbf{S}_R\|_2^2 \leq \frac{(C_2 - c) \sum_k A_{k,R}^2}{2} \right\} \leq 2 \exp \left(-\frac{c_0}{64} (C_2 - c) \right). \quad (99)$$

Similarly, we have

$$\mathbb{P} \left\{ \|\mathbf{Q}\mathbf{S}_I\|_2^2 \leq \frac{(C_2 - c) \sum_k A_{k,I}^2}{2} \right\} \leq 2 \exp \left(-\frac{c_0}{64} (C_2 - c) \right). \quad (100)$$

Since \mathbf{Q} is a real-valued matrix, $\|\mathbf{Q}\mathbf{S}\|_2^2 = \|\mathbf{Q}\mathbf{S}_R\|_2^2 + \|\mathbf{Q}\mathbf{S}_I\|_2^2$. Moreover, $\sum_k |A_{k,b}|^2 = \sum_k (A_{k,R}^2 + A_{k,I}^2)$.

Combining (99) and (100), we have

$$\mathbb{P} \left\{ \|\mathbf{Q}\mathbf{S}\|_2^2 \leq \frac{(C_2 - c) \sum_k |A_{k,b}|^2}{2} \right\} \leq \mathbb{P} \left\{ \|\mathbf{Q}\mathbf{S}_R\|_2^2 \leq \frac{(C_2 - c) \sum_k A_{k,R}^2}{2} \right\} + \mathbb{P} \left\{ \|\mathbf{Q}\mathbf{S}_I\|_2^2 \leq \frac{(C_2 - c) \sum_k A_{k,I}^2}{2} \right\} \quad (101)$$

$$\leq 4 \exp \left(-\frac{c_0}{64} (C_2 - c) \right). \quad (102)$$

Combining (83), (86) and (102), there exists some large enough β_1 such that $C_2 = \beta_1 \lceil \log N \rceil$ and

$$\mathbb{P} \{ \|\mathbf{Q}\mathbf{S} + \mathbf{Z}\|_2^2 \leq \eta \} \leq \frac{2}{K^2}. \quad (103)$$

We can write the error probability that asingleton bin is declared as a zero-ton as

$$\mathbb{P} \{ E_{b,1,0} \} = \mathbb{P} \left\{ \|A_{k,b} \dot{\mathbf{g}}_k + \dot{\mathbf{Z}}_b\|_2^2 \leq \eta \right\}. \quad (104)$$

Therefore, we can apply Lemma 2 with $\mathbf{S} = A_{k,b} \dot{\mathbf{g}}_k$, $\mathbf{Q} = \mathbf{I}$, $\mathbf{Z} = \dot{\mathbf{Z}}_b$ and $k_0 = 1$ to obtain (55).

APPENDIX B
PROOF OF MULTITON ERROR

We rewrite the bin values as follows,

$$\dot{\mathbf{Y}}_b = \sum_{k \in \mathcal{K}: b \in \mathcal{B}_k} A_{k,b} \dot{\mathbf{g}}_k + \dot{\mathbf{Z}}_b, \quad (105)$$

where $\dot{\mathbf{Z}}_b = \dot{\mathbf{W}}_b + \dot{\mathbf{V}}_b$.

Suppose the incorrect estimate index from bin b is k_b . We have

$$\dot{A}_{k_b} = \sum_{k \in \mathcal{K}: b \in \mathcal{B}_k} \frac{1}{C_2} A_{k,b} \dot{\mathbf{g}}_{k_b}^\dagger \dot{\mathbf{g}}_k + \frac{1}{C_2} \dot{\mathbf{g}}_{k_b}^\dagger \dot{\mathbf{Z}}_b. \quad (106)$$

Thus,

$$\dot{\mathbf{Y}}_b - \dot{A}_{k_b} \dot{\mathbf{g}}_{k_b} = \sum_{k \in \mathcal{K}: b \in \mathcal{B}_k} A_{k,b} \left(\mathbf{I} - \frac{\dot{\mathbf{g}}_{k_b} \dot{\mathbf{g}}_{k_b}^\dagger}{C_2} \right) \dot{\mathbf{g}}_k + \left(\mathbf{I} - \frac{\dot{\mathbf{g}}_{k_b} \dot{\mathbf{g}}_{k_b}^\dagger}{C_2} \right) \dot{\mathbf{Z}}_b. \quad (107)$$

Let

$$\mathbf{S} = \sum_{k \in \mathcal{K}: b \in \mathcal{B}_k} A_{k,b} \dot{\mathbf{g}}_k \quad (108)$$

and $\mathbf{Q} = \mathbf{I} - \frac{1}{C_2} \dot{\mathbf{g}}_{k_b} \dot{\mathbf{g}}_{k_b}^\dagger$, then the first term in (107) can be written as

$$\sum_{k \in \mathcal{K}: b \in \mathcal{B}_k} A_{k,b} \left(\mathbf{I} - \frac{\dot{\mathbf{g}}_{k_b} \dot{\mathbf{g}}_{k_b}^\dagger}{C_2} \right) \dot{\mathbf{g}}_k = \mathbf{Q} \mathbf{S}. \quad (109)$$

The multiton bin cannot be detected when $\|\mathbf{Y}_b - \dot{A}_{k_b,b} \dot{\mathbf{g}}_{k_b}\|_2^2 \leq \eta$. In the following, we upper bound the error probability assuming $k_b \notin \{k \in \mathcal{K} : b \in \mathcal{B}_k\}$. A similar analysis can be carried out for the case of $k_b \in \{k \in \mathcal{K} : b \in \mathcal{B}_k\}$. Conditioned on $\dot{\mathbf{g}}_{k_b}$, we can apply Lemma 2 with $c = 1$, $k_0 = |k \in \mathcal{K} : b \in \mathcal{B}_k|$ and $\mathbf{Z} = \mathbf{Q} \dot{\mathbf{Z}}_b$ to upper bound the error probability as

$$\mathbb{P} \left\{ \|\mathbf{Y}_b - \dot{A}_{k_b,b} \dot{\mathbf{g}}_{k_b}\|_2^2 \leq \eta \mid \dot{\mathbf{g}}_{k_b} \right\} = \mathbb{P} \left\{ \|\mathbf{Q} \mathbf{S} + \mathbf{Q} \dot{\mathbf{Z}}_b\|_2^2 \leq \eta \mid \dot{\mathbf{g}}_{k_b} \right\} \quad (110)$$

$$\leq \frac{2}{K^2}. \quad (111)$$

Since (110) holds for all $\dot{\mathbf{g}}_{k_b}$, we have

$$\mathbb{P} \left\{ \|\mathbf{Y}_b - \dot{A}_{k_b,b} \dot{\mathbf{g}}_{k_b}\|_2^2 \leq \eta \right\} \leq \frac{2}{K^2}. \quad (112)$$

APPENDIX C
PROOF OF LEMMA 1

We focus on the delay estimation for device k . Without loss of generality, we assume the delay is $m_k = 0$. The device experiences the interference from the other $K - 1$ devices and noise. The received synchronization pilots

can be written as

$$y_i = a_k s_{k,i} + z_i, \quad (113)$$

where the time-domain samples of the pilots $s_{k,i} \sim \mathcal{CN}(0, 1)$ and $z_i \sim \mathcal{CN}(0, 2\sigma_z^2)$, where the variance is bounded as

$$(K-1)\underline{a}^2 + 2\sigma^2 \leq 2\sigma_z^2 \leq (K-1)\bar{a}^2 + 2\sigma^2. \quad (114)$$

Let \mathcal{I} be given by (16). The number of samples contained in \mathcal{I} is $|\mathcal{I}| = BC_3$. According to (17), The test metric is calculated as

$$\mathcal{T}(m) = \sum_{i \in \mathcal{I}} a_k s_{k,i+m} s_{k,i}^* + z_{i+m} s_{k,i}^*. \quad (115)$$

When the delay is correctly estimated, the test metric given by (17) is calculated as

$$\mathcal{T}(0) = BC_3 a_k + \sum_{i \in \mathcal{I}} z_i s_{k,i}^*. \quad (116)$$

By the central limit theorem, $\mathcal{T}(0) \sim \mathcal{CN}(BC_3 a_k, KBC_3 \sigma_0^2)$ and $\mathcal{T}(m) \sim \mathcal{CN}(0, KBC_3 \sigma_m^2)$, where σ_0 and σ_m are some bounded constants independent of K .

We define a threshold $\bar{\mathcal{T}} = \underline{a}BC_3/2$. If $|\mathcal{T}(0)| > \bar{\mathcal{T}}$ and $|\mathcal{T}(m)| < \bar{\mathcal{T}}$ for all $m = 1, \dots, M$, the delay can be correctly estimated. Therefore, the error probability can be upper bounded as

$$P_e \leq \sum_{m=1}^M \mathbb{P}\{|\mathcal{T}(m)| \geq \bar{\mathcal{T}}\} + \mathbb{P}\{|\mathcal{T}(0)| \leq \bar{\mathcal{T}}\}. \quad (117)$$

The first term can be upper bounded as

$$\mathbb{P}\{|\mathcal{T}(m)| \geq \bar{\mathcal{T}}\} \leq \mathbb{P}\{|\operatorname{Re}\{\mathcal{T}(m)\}| \geq \bar{\mathcal{T}}/2\} + \mathbb{P}\{|\operatorname{Im}\{\mathcal{T}(m)\}| \geq \bar{\mathcal{T}}/2\} \quad (118)$$

$$\leq 4\mathbb{P}\left\{\mathcal{N}\left(0, \frac{KBC_3\sigma_m^2}{2}\right) \geq \frac{\underline{a}BC_3}{4}\right\} \quad (119)$$

$$\leq 4e^{-\frac{\underline{a}^2 BC_3}{16\sigma_m^2 K}}. \quad (120)$$

Let ϕ be the phase of a_k . The second term in (117) can be upper bounded as

$$\mathbb{P}\{|\mathcal{T}(0)| \leq \bar{\mathcal{T}}\} = \mathbb{P}\{|a_k|BC_3 + e^{-j\phi} \sum_{i \in \mathcal{I}} z_i s_i^* \leq \bar{\mathcal{T}}\} \quad (121)$$

$$\leq \mathbb{P}\left\{\mathcal{N}\left(|a_k|BC_3, \frac{KBC_3\sigma_0^2}{2}\right) \leq \frac{\underline{a}BC_3}{2}\right\} \quad (122)$$

$$\leq Q\left(\sqrt{\frac{\underline{a}^2 BC_3}{2\sigma_0^2 K}}\right) \quad (123)$$

$$\leq e^{-\frac{\underline{a}^2 BC_3}{4\sigma_0^2 K}}. \quad (124)$$

Combining (117), (120) and (124), given that $B = \beta_0 K$, there exists some β_4 such that $C_3 = \beta_4 \lceil \log(K+M) \rceil$

and the error probability of delay estimation is less than $1/K^2$.

APPENDIX D

AUXILIARY RESULTS ON SUB-GAUSSIAN VARIABLES

The following lemmas and theorem are established in [40].

Lemma 4: Suppose X is σ -subGaussian, then aX is $a\sigma$ -subGaussian.

Lemma 5: Suppose X_1 is σ_1 -subGaussian, X_2 is σ_2 -subGaussian. Moreover, they are independent. Then $X_1 + X_2$ is $\sqrt{\sigma_1^2 + \sigma_2^2}$ -subGaussian.

Theorem 3 (Characterization of subGaussian variables): Let $EX = 0$. The following are equivalent:

- 1) $E(e^{tX}) \leq e^{\frac{t^2}{4}}$.
- 2) $\forall t > 0, P\{|X| > t\} \leq 2\exp(-t^2)$.
- 3) $\forall p \geq 1, (E|X|^p)^{1/p} \leq \sqrt{2p}$.

The following theorem is on the concentration of subGaussian random variables.

Theorem 4 (Hanson-Wright inequality [41]): Let $\mathbf{Z} = (Z_1, \dots, Z_n) \in \mathbb{R}^n$ be a random vector with independent components Z_i which satisfy $EZ_i = 0$ and the subGaussian norm $\|Z_i\|_{\phi_2} \leq K$. Let \mathbf{A} be an $n \times n$ matrix. Then, for every $t \geq 0$,

$$P\left\{|\mathbf{Z}^T \mathbf{A} \mathbf{Z} - E\{\mathbf{Z}^T \mathbf{A} \mathbf{Z}\}| > t\right\} \leq 2 \exp\left[-c_0 \min\left(\frac{t^2}{K^4 \|\mathbf{A}\|_F^2}, \frac{t}{K^2 \|\mathbf{A}\|}\right)\right],$$

where the operator norm of \mathbf{A} is $\|\mathbf{A}\| = \max_{\mathbf{x} \neq 0} \frac{\|\mathbf{A}\mathbf{x}\|_2}{\|\mathbf{x}\|_2}$, the Frobenius norm of \mathbf{A} is $\|\mathbf{A}\|_F = (\sum_{i,j} |A_{i,j}|^2)^{1/2}$ and c_0 is some positive constant.

REFERENCES

- [1] C. MacGillivray, V. Turner, and D. Lund, "Worldwide Internet of Things (IoT) 2013–2020 forecast: Billions of things, trillions of dollars," *Market Analysis*, vol. 243661, 2013.
- [2] M. J. McGlynn and S. A. Borbash, "Birthday protocols for low energy deployment and flexible neighbor discovery in ad hoc wireless networks," in *Proc. ACM MobiHoc*, Long Beach, CA, 2001, pp. 137–145.
- [3] S. Vasudevan, D. Towsley, D. Goeckel, and R. Khalili, "Neighbor discovery in wireless networks and the coupon collector's problem," in *Proc. ACM Mobicom*, Beijing, China, 2009, pp. 181–192.
- [4] D. Angelosante, E. Biglieri, and M. Lops, "Neighbor discovery in wireless networks: a multiuser-detection approach," *Physical Communication*, vol. 3, no. 1, pp. 28–36, 2010.
- [5] X. Chen and D. Guo, "Many-access channels: The Gaussian case with random user activities," in *Proc. IEEE Int. Symp. Information Theory*, Honolulu, HI, June 2014, pp. 3127–3131.
- [6] M. Z. Shafiq, L. Ji, A. X. Liu, J. Pang, and J. Wang, "A first look at cellular machine-to-machine traffic: large scale measurement and characterization," in *ACM SIGMETRICS Performance Evaluation Review*, vol. 40, no. 1, 2012, pp. 65–76.
- [7] S. A. Borbash, A. Ephremides, and M. J. McGlynn, "An asynchronous neighbor discovery algorithm for wireless sensor networks," *Ad Hoc Networks*, vol. 5, no. 7, pp. 998–1016, 2007.
- [8] S. Vasudevan, J. Kurose, and D. Towsley, "On neighbor discovery in wireless networks with directional antennas," in *Proc. IEEE INFOCOM*, vol. 4, Miami, FL, March 2005, pp. 2502–2512.
- [9] S. Chen, A. Russell, R. Jin, Y. Qin, B. Wang, and S. Vasudevan, "Asynchronous neighbor discovery on duty-cycled mobile devices: Integer and non-integer schedules," in *Proc. ACM MobiHoc*, Hangzhou, China, 2015, pp. 47–56.
- [10] J. Ni, R. Srikant, and X. Wu, "Coloring spatial point processes with applications to peer discovery in large wireless networks," *IEEE/ACM Trans. Networking*, vol. 19, no. 2, pp. 575–588, 2011.

- [11] X. Wu, S. Tavildar, S. Shakkottai, T. Richardson, J. Li, R. Laroia, and A. Jovicic, "Flashlinq: A synchronous distributed scheduler for peer-to-peer ad hoc networks," *IEEE/ACM Trans. Networking*, vol. 21, no. 4, pp. 1215–1228, 2013.
- [12] E. Paolini, G. Liva, and M. Chiani, "Coded slotted ALOHA: A graph-based method for uncoordinated multiple access," *IEEE Trans. Inf. Theory*, vol. 61, no. 12, pp. 6815–6832, 2015.
- [13] A. Taghavi, A. Vem, J.-F. Chamberland, and K. Narayanan, "On the design of universal schemes for massive uncoordinated multiple access," in *Proc. IEEE Int. Symp. Information Theory*, Barcelona, Spain, July 2016.
- [14] R. De Gaudenzi, O. del Rio Herrero, G. Acar, and E. G. Barrabés, "Asynchronous contention resolution diversity aloha: Making crdsa truly asynchronous," *IEEE Trans. on Wireless Commun.*, vol. 13, no. 11, pp. 6193–6206, 2014.
- [15] F. Clazzer, F. Lazaro, G. Liva, and M. Marchese, "Detection and combining techniques for asynchronous random access with time diversity," *arXiv preprint arXiv:1604.06221*, 2016.
- [16] E. Sandgren, F. Brännström *et al.*, "On frame asynchronous coded slotted aloha: Asymptotic, finite length, and delay analysis," *arXiv preprint arXiv:1606.03242*, 2016.
- [17] M. Shirvanimoghaddam, Y. Li, M. Dohler, B. Vucetic, and S. Feng, "Probabilistic rateless multiple access for machine-to-machine communication," *IEEE Trans. on Wireless Commun.*, vol. 14, no. 12, pp. 6815–6826, 2015.
- [18] H. Zhu and G. B. Giannakis, "Exploiting sparse user activity in multiuser detection," *IEEE Trans. on Commun.*, vol. 59, no. 2, pp. 454–465, 2011.
- [19] H. F. Schepker and A. Dekorsy, "Compressive sensing multi-user detection with block-wise orthogonal least squares," in *Proc. IEEE Veh. Tech. Conf.*, Yokohama, Japan, 2012, pp. 1–5.
- [20] L. Zhang, J. Luo, and D. Guo, "Neighbor discovery for wireless networks via compressed sensing," *Performance Evaluation*, vol. 70, no. 7, pp. 457–471, 2013.
- [21] L. Zhang and D. Guo, "Virtual full duplex wireless broadcasting via compressed sensing," *IEEE/ACM Trans. Networking*, vol. 22, no. 5, pp. 1659–1671, 2014.
- [22] L. Liu and W. Yu, "Massive connectivity with massive MIMO-part I: Device activity detection and channel estimation," *arXiv preprint arXiv:1706.06438*, 2017.
- [23] L. Applebaum, W. U. Bajwa, M. F. Duarte, and R. Calderbank, "Asynchronous code-division random access using convex optimization," *Physical Communication*, vol. 5, no. 2, pp. 129–147, 2012.
- [24] J. Luo and D. Guo, "Neighbor discovery in wireless ad hoc networks based on group testing," in *Proc. Annual Allerton Conference on Commun., Control, and Computing*, Monticello, IL, 2008, pp. 791–797.
- [25] K. Chandrasekher, K. Lee, P. Kairouz, R. Pedarsani, and K. Ramchandran, "Asynchronous and noncoherent neighbor discovery for the IoT using sparse-graph codes," in *Proc. IEEE Int. Conf. Commun.*, Paris, France, May 2017.
- [26] S. Pawar and K. Ramchandran, "Computing a k -sparse n -length discrete Fourier transform using at most $4k$ samples and $O(k \log k)$ complexity," in *Proc. IEEE Int. Symp. Inform. Theory*, Istanbul, 2013, pp. 464–468.
- [27] X. Chen and D. Guo, "Robust sublinear complexity Walsh Hadamard transform with arbitrary sparse support," in *Proc. IEEE Int. Symp. Information Theory*, Hong Kong, June 2015.
- [28] S. Pawar and K. Ramchandran, "A hybrid DFT-LDPC framework for fast, efficient and robust compressive sensing," in *Proc. Annual Allerton Conference on Commun., Control, and Computing*, Monticello, IL, 2012, pp. 1943–1950.
- [29] X. Li, J. K. Bradley, S. Pawar, and K. Ramchandran, "The SPRIGHT algorithm for robust sparse Hadamard transforms," in *Proc. IEEE Int. Symp. Inform. Theory*, Honolulu, HI, 2014, pp. 1857–1861.
- [30] W. Zeng, S. Vasudevan, X. Chen, B. Wang, A. Russell, and W. Wei, "Neighbor discovery in wireless networks with multipacket reception," in *Proc. ACM MobiHoc*, Paris, France, 2011, p. 3.
- [31] J. Jeon and A. Ephremides, "Neighbor discovery in a wireless sensor network: Multipacket reception capability and physical-layer signal processing," *J. Commun. Networks*, vol. 14, no. 5, pp. 566–577, 2012.
- [32] M. J. Wainwright, "Information-theoretic limits on sparsity recovery in the high-dimensional and noisy setting," *IEEE Trans. Inf. Theory*, vol. 55, no. 12, pp. 5728–5741, 2009.
- [33] X. Chen and D. Guo, "A generalized LDPC framework for sublinear compressive sensing," in *Proc. IEEE Int. Conf. Acoustics, Speech, and Signal Processing*, Shanghai, China, March 2016.
- [34] A. Barg and G. Zémor, "Error exponents of expander codes under linear-complexity decoding," *SIAM J. on Discrete Math.*, vol. 17, no. 3, pp. 426–445, 2004.

- [35] S. Pawar and K. Ramchandran, “A robust R-FFAST framework for computing a k -sparse n -length DFT in $O(k \log n)$ sample complexity using sparse-graph codes,” in *Proc. IEEE Int. Symp. Inform. Theory*, Honolulu, HI, June 2014, pp. 1852–1856.
- [36] X. Li, S. Pawar, and K. Ramchandran, “Sub-linear time compressed sensing using sparse-graph codes,” in *Proc. IEEE Int. Symp. Information Theory*, Hong Kong, 2015, pp. 1645–1649.
- [37] E. Price, “Efficient sketches for the set query problem,” in *Proceedings of the Twenty-Second Annual ACM-SIAM Symposium on Discrete Algorithms*, San Francisco, California, 2011, pp. 41–56.
- [38] M. Karoński and T. Łuczak, “The phase transition in a random hypergraph,” *Journal of Computational and Applied Mathematics*, vol. 142, no. 1, pp. 125–135, 2002.
- [39] J. Schmidt-Pruzan and E. Shamir, “Component structure in the evolution of random hypergraphs,” *Combinatorica*, vol. 5, no. 1, pp. 81–94, 1985.
- [40] O. Rivasplata, “Subgaussian random variables: an expository note,” *Internet publication, PDF*, 2012.
- [41] M. Rudelson and R. Vershynin, “Hanson-wright inequality and sub-gaussian concentration,” *Electronic Communications in Probability*, vol. 18, pp. 1–9, 2013.